THE HOST ROCK OF THE CENTRAL PATAGONIAN BATHOLITH IN GASTRE: FURTHER INSIGHTS ON THE LATE TRIASSIC TO EARLY JURASSIC DEFORMATION IN THE REGION

Claudia Beatriz ZAFFARANA[1, 2], Teresita MONTENEGRO[1, 2] y Rubén SOMOZA[1, 2]

[1] Consejo Nacional de Investigaciones Científicas y Técnicas (CONICET)
[2] Departamento de Ciencias Geológicas, Facultad de Ciencias Exactas y Naturales, Universidad de Buenos Aires

ABSTRACT

Small outcrops of biotitic-amphibolic schists and amphibolites found in two localities suggest that the Cushamen Formation is host rock of the Central Patagonian Batholith in Gastre. The characteristics of these rocks were investigated using structural, petrographic, magnetic fabric, and garnet chemical-zonation studies. Garnet is observed as a late product of contact metamorphism. Structural data from the studied area and from other localities in the region are in conflict with models that invoke the occurrence of uniform, large-scale dextral displacements along the Gastre lineament in Mesosoic times. Rather, the data suggest that the Gastre granitoids record heterogeneous low-temperature deformation of likely Late Triassic age. This low-temperature deformation appears as small, localized outcrops, and we suggest that it is related to the accommodation of the successive magma batches that built the Central Patagonian Batholith.

Keywords: *Gastre, Gastre Fault System, North-Patagonian Massif, Central Patagonian Batholith, basement rocks, garnet zonation.*

RESUMEN

La roca de caja del Batolito de la Patagonia Central en Gastre: nuevas evidencias sobre la deformación del Triásico tardío - Jurásico temprano en la región.
El hallazgo de dos pequeños afloramientos de esquistos biotítico-anfibólicos y de anfibolitas en dos localidades sugiere que la Formación Cushamen es roca de caja del Batolito de la Patagonia Central en Gastre. Las características de estas rocas metamórficas fueron analizadas mediante estudios petrográficos, microestructurales, de fábrica magnética y de zonación química de granates. Los resultados indican que el granate es producto tardío de metamorfismo de contacto. Los datos estructurales en las localidades estudiadas y en otras áreas de la región no condicen con los modelos de deformación homogénea de transcurrencia dextral propuestos para el sistema de Fallas de Gastre durante el Mesozoico. En cambio, los datos sugieren que la deformación en estado sólido que muestran los granitoides es local y heterogénea, y con posible edad triásica tardía. Nosotros relacionamos esta deformación de baja temperatura con el acomodamiento de los sucesivos pulsos magmáticos que construyeron el Batolito de la Patagonia Central.

Palabras clave: *Gastre, sistema de Fallas de Gastre, Macizo Norpatagónico, Batolito de la Patagonia Central, rocas de basamento, zonación en granate.*

INTRODUCTION

The Central Patagonian Batholith (CPB, Fig. 1) comprises a suite of NW-SE trending, Late Triassic granitoids attributed to the early stages of arc-related magmatism in the Mesozoic-Cenozoic history of the North Patagonian Massif (Rapela *et al.* 1991, 1992, Rapela and Pankhurst 1992). Contrasting with the large area occupied by the batholith in the Sierra de Calcatapul (Fig. 1), its unique recognized metamorphic host rock, the Calcatapul Formation (Proserpio 1978), is represented by rather small outcrops in two localities (Fig. 1, Fig. 2). The Calcatapul Formation consists of a metamorphic succession of various metavolcanic rocks along with thin layers of phyllites and lenses of metaconglomerates (von Gosen and Loske 2004, Zaffarana *et al.* 2010) and it also shows signs of dynamic metamorphism. In the northern sector of the Sierra del Medio, several kilometers WNW from the outcrops of the Calcatapul Formation (Fig. 1), the granitoids of the Central Patagonian Batholith intrude the Mamil Choique Granitoids (e.g. Rapela *et al.* 1991, 1992), which represent the widespread, Late Paleozoic plutonism in the North

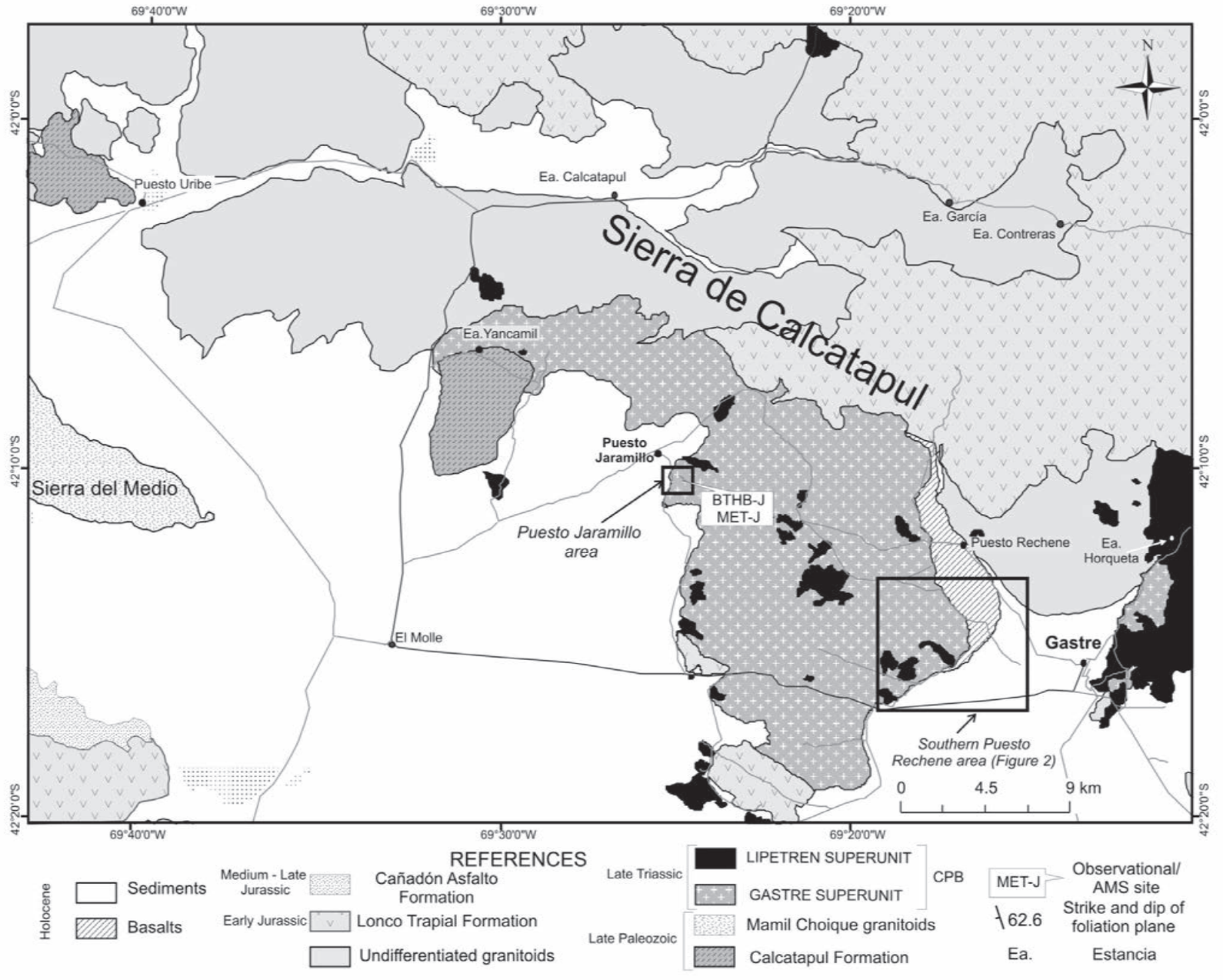

Figure 1: Geologic map of the Central Patagonian Batholith (CPB) in the Gastre area, western sector of the North Patagonian Massif, extracted from Zaffarana *et al.* (2010) and Zaffarana (2011). Formal name of units compiled from Proserpio (1978), Rapela *et al.* (1992) and Figari *et al.* (1994).

Patagonian Massif (e.g. Pankhurst *et al.* 2006). Recently, von Gosen and Loske (2004) reported an age of ~272 Ma (U/Pb conventional method) for the Yancamil granite, which intrudes the Calcatapul Formation at Estancia Yancamil (Fig. 1) and in turn is intruded by the Central Patagonian Batholith. This granite was previously mapped as part of the Central Patagonian Batholith, suggesting the possibility that other outcrops of yet unrecognized Late Paleozoic plutons host the Central Patagonian Batholith elsewhere.

In this contribution we report the characteristics of newly found, small (not mappable) outcrops of host rock from the Central Patagonian Batholith in, or very close to the village of Gastre. These outcrops are metasedimentary rocks which appear as a xenolith in Puesto Jaramillo (42º 10.662´S, 69º 24.864´W, Fig. 2) and small septums of biotitic and amphibolic schists and amphibolites in Puesto Rechene (42º 15.246´S, 69º 17.19´W, Fig. 2). We assume that these rocks belong to the Cushamen Formation (Volkheimer 1964). In this contribution we named as xenolith to an isolated piece of host rock that could not have remained in place after the intrusion. On the other hand, a septum (or raft, following Pignotta *et al.* 2010) is considered as a host rock xenolith that is surrounded by plutonic material and where no discernable rotation and/or translation (relative to in situ host rock) of the enclave can be demonstrated. Septums are usually thin wall or roof pendants, those that we saw are at least two orders of magnitude larger than the xenoliths.

In order to have as complete as possible information about the characteristics of these previously unnoticed basement rocks in Gastre, this report includes structural, petrographic, magnetic fabrics, and garnet chemical-zonation analyses. Each of these items is presented with a brief methodological introduction which is followed by a presentation of the results. Finally, the entire dataset is integrated in order to enlarge as much as possible the information on the newly discovered outcrops of the host rock from the Central Patagonian Batholith. In particular, the structural information from this paper together with structural information from previous contributions is analyzed in the context of the deformational predictions of the so-called Gastre Fault System model. The structural, anisotropy of the magnetic susceptibility (AMS) and chemical data from the new outcrops are listed in the appendix.

GEOLOGICAL OVERVIEW

A set of granitoids crops out in the area of Gastre, in the central sector of the North Patagonian Massif. These granitoids can be broadly divided in two groups: an older one composed of biotite and hornblende granodiorites, diorites, monzodiorites, granites and monzogranites, and a younger magmatic pulse mostly represented by red-colored, fine-grained biotitic granites. Proserpio (1978) associated the older set of granitoids with the Mamil Choique Formation (Ravazzoli and Sesana 1977), or Mamil Choique Granitoids (Dalla Salda *et al.* 1994) and the younger ones with the Lipetrén Formation, which was defined by Nullo (1979) in the Sierra de Lipetrén, north of Gastre. The type locality of the Mamil Choique Granitoids is the Rio Chico-Mamil Choique area (between 41º 40´ and 41º 55´S and 70º 00´ and 70º 33´W), where they are composed of three peraluminous facies: the biotite ± muscovite ± hornblende ± epidote tonalite-granodiorite, biotite-muscovite monzogranites, as well as by intrusive, partially porphyritic biotite-muscovite monzogranites (Cerredo and López de Luchi 1998, López de Luchi and Cerredo 2008). Their various isotopic ages span from Late Devonian to Permian (Linares *et al.* 1997, López de Luchi *et al.* 2000, Varela *et al.* 2005). The emplacement of the two older facies has been ascribed to deep- to mid-crustal processes related with decompression after the climax of regional metamorphism in their hosting Cushamen Formation, whereas the later monzongranite intrusion could have occurred at upper crustal levels (Cerredo and López de Luchi 1998, López de Luchi and Cerredo 2008). In a more regional view, the Mamil Choique Granitoids are part of the extended Permian magmatism of the North Patagonian Massif recently described by Pankhurst *et al.* (2006).

The geochemical and geochronological studies performed by Rapela *et al.* (1991, 1992) revealed that most of the granitoids of the Gastre area comprise a batholith of predominantly Late Triassic age (the Central Patagonian Batholith, CPB). This batholith (Fig. 1) is composed of the older Gastre Superunit (~220 Ma Rb/Sr age, Rapela *et al.* 1992), a younger Lipetrén Superunit (~210 Ma Rb/sr age, Rapela *et al.* 1992) plus a separated small stock named Horqueta granodiorite previously thought to be Jurassic (Rb/Sr, Rapela *et al.* 1992) and from which we recently obtained a ~214 Ma age (^{40}Ar-^{39}Ar, biotite), and therefore include it into the Lipetrén Superunit. In this new scheme, the Paleozoic Mamil Choique granitoids were restricted to the Sierra del Medio area and to the Laguna del Toro (Sierra de Taquetrén) areas, which are located to the west and south of Gastre, respectively, both nearby but out of the area enclosed in Fig. 1. The Laguna del Toro granitoids are tonalites and two-mica granitoids (Rapela *et al.* 1992), and the Sierra del Medio granitoids are mostly tonalites and granites (Llambías *et al.* 1984).

The Late Triassic granitoids of the Central Patagonian Batholith have a calc-alkaline I-type geochemistry, although their initial ^{87}Sr/^{86}Sr ratios and ξNdt values point to "modified I-type" magmas generated in a continental magmatic arc setting (Rapela *et al.* 1991, 1992, Rapela and Pankhurst 1992). Their emplacement would have been controlled by the activity of the Gastre Fault System, a set of NW-SE subvertical lineaments which pass through the Gastre area (Coira *et al.* 1975). Overlying the granitoids there is the Lonco Trapial Formation (Page and Page, 1993, Zaffarana and Somoza 2012), a volcano-sedimentary unit from which we

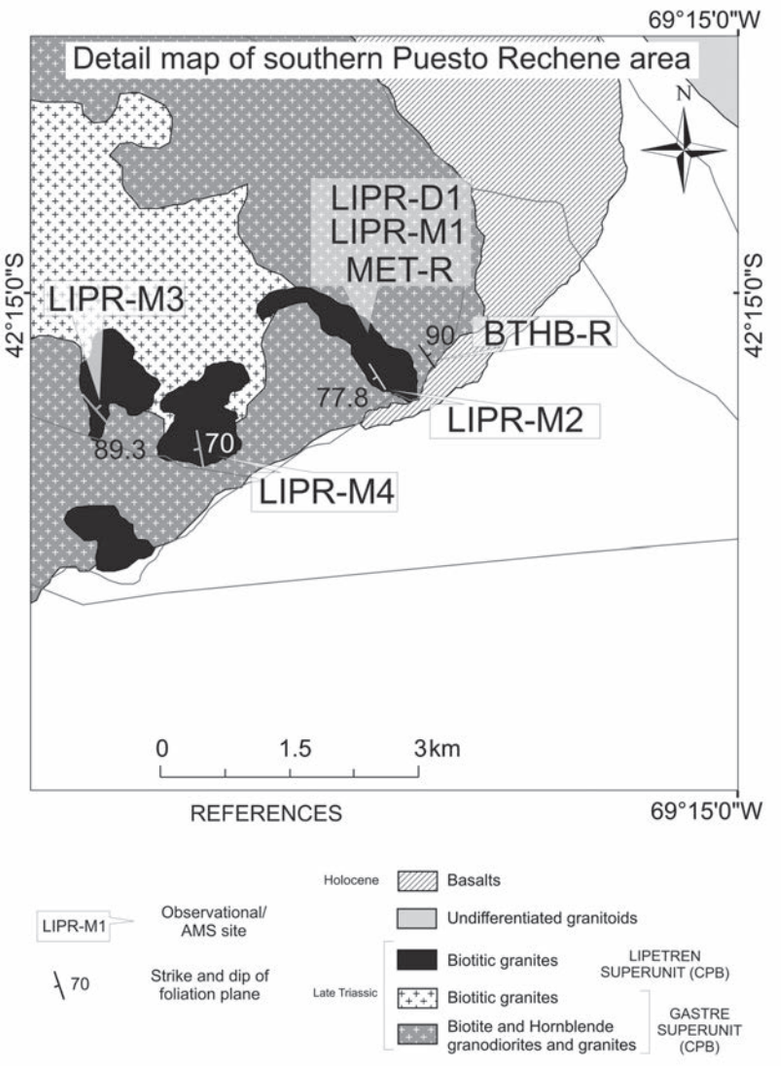

Figure 2: Detailed map of the study area extracted from Zaffarana *et al.* (2010). The foliation planes drawn in this map represent field data in sites BTHB-R and LIPR-M4 and magnetic foliation data in sites MET-R, LIPR-D1, LIPR-M1, LIPR-M2 and LIPR-M3 (see the text for further explanations).

recently obtained Karoo-like (Early Jurassic) $^{40}Ar/^{39}Ar$ ages. The Lonco Trapial unit is not affected by the low-temperature deformation observed in the Central Patagonian Batholith (Zaffarana *et al.*, 2010), placing an upper temporal bound to the deformational event that affects the Late Triassic granitoids.

Nearby the area enclosed in figure 1, the older Paleozoic granitoids were restricted to the Sierra del Medio area and to the Laguna del Toro (Sierra de Taquetrén) areas, which are located to the west and south of Gastre, respectively. The Laguna del Toro granitoids are tonalites and two-mica granitoids (Rapela *et al.* 1992), and the Sierra del Medio granitoids are mostly tonalites and granites (Llambías *et al.* 1984).

The outcrops of metamorphic basement in the North Patagonian Massif are grouped into the Cushamen Formation (Volkheimer 1964), which is well exposed in the Comallo and Río Chico areas. The Cushamen Formation comprises phyllites, quartzite layers, (injected) micaschists, amphibolites, gneisses and migmatites (Volkheimer 1964, Volkheimer and Lage 1981, Dalla Salda *et al.* 1994, Duhart *et al.* 2002, Giacosa *et al.* 2004, among many others). Cerredo and López de Luchi (1999) and López de Luchi *et al.* (2002) further report the presence of metavolcanic rocks as dikes and very thin intercalations of lavas in the Cushamen Formation. The protolith ages of the Cushamen Formation could be Late Paleozoic (Duhart *et al.* 2002) and in parts might be older (Linares *et al.* 1988, 1997, Ostera *et al.* 2001, Hervé *et al.* 2005). The metamorphism of the Cushamen Formation is bracketed in time between the Visean (335 Ma) and the Early Permian (Hervé *et al.* 2005). Thin screens and xenoliths of the Cushamen Formation are hosted by the Mamil Choique Granitoids in the Rio Chico area (López de Luchi *et al.* 2002, López de Luchi and Cerredo 2008).

In the Gastre area, the only known basement rocks were grouped into the Calcatapul Formation (Proserpio 1978), which consists of a metamorphic succession of acid and basic metavolcanic rocks along with thin intercalations of phyllites and lenses of metaconglomerates and shows signs of dynamic metamorphism (Proserpio 1978, von Gosen and Loske 2004, Zaffarana *et al.* 2010). The Calcatapul Formation acquired its S_1 tectonic foliation at a slightly lower metamorphic grade (greenschist facies conditions) than the Cushamen Formation, whose metamorphic grade, though variable, reached upper amphibolite facies (Dalla Salda *et al.* 1994, López de Luchi and Cerredo 1998). The tectonic foliation S_1 of the Calcatapul Formation is parallel to the magmatic to solid-state foliation of the intruding granitoids at Estancia Yancamil (von Gosen and Loske 2004, Zaffarana *et al.* 2010), suggesting that both lithologies acquired their foliations simultaneously during (and slightly after) the time of pluton emplacement. No folds were found in the Calcatapul Formation strata, neither at Puesto Yancamil nor at Puesto Uribe.

FIELD AND PETROGRAPHIC CHARACTERISTICS

The criteria of Paterson *et al.* (1989, 1998) were followed to distinguish between

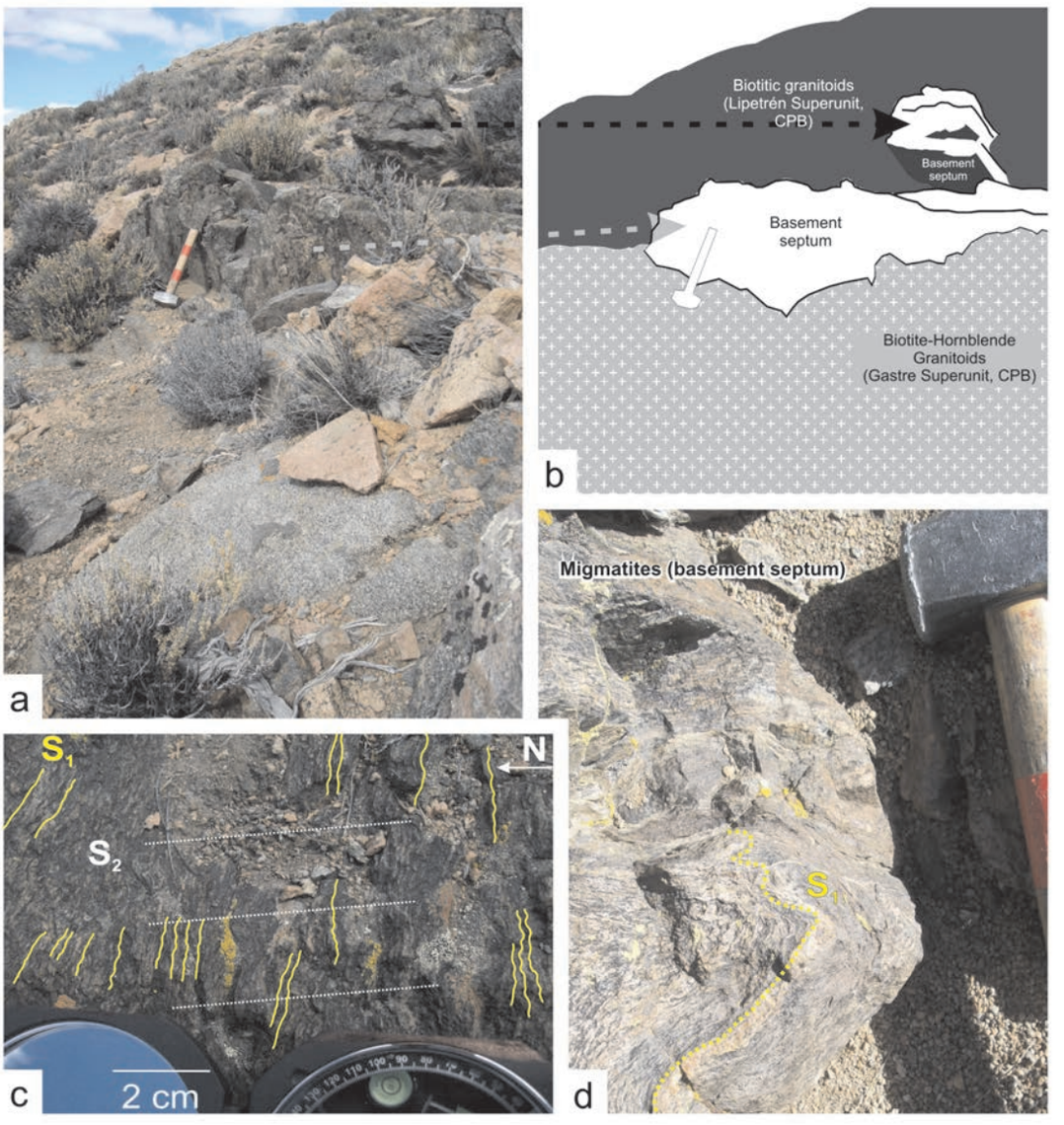

Figure 3: Field appearance of the basement rocks in southern Puesto Rechene area (Fig. 2) a) Biotitic/amphibolic schists septums with NW-SE subvertical orientation in the contact between two different facies of the Central Patagonian Batholith (CPB). b) Scheme of a. c) Superimposition of two deformations in the basement rocks: S1 foliation planes with E-W subvertical orientation and S2 axial surface of NW-SE subvertical orientation. d) Stromatitic migmatites within the basement rocks. CPB: Central Patagonian Batholith.

magmatic and tectonic foliations in granitoids. The in force of this methodology is highlighted by its application in many recent articles on petrology and structural geology of igneous rocks (e.g. Žák *et al.* 2005, 2006, 2007, Paterson 2009, Yoshinobu *et al.* 2009, Pignotta *et al.* 2010). Temperature of acquisition of both fabrics and microstructures was estimated according to the extensive literature available on the subject (see references within Passchier and Trouw 2005 and Vernon 2004).

South of Puesto Rechene area

Metamorphic rocks: a small outcrop of dark-coloured biotitic-amphibolic schists and amphibolites appears as 10s of meters scale septums interspersed between the granitoids of the Central Patagonian Batholith in the area south of Puesto Rechene (Figs. 1 and 2). The contacts between the metamorphic rocks and the granitoids are sharp and clear. The septums of metamorphic rocks are tabular and have a NW-SE subvertical orientation (Fig. 3a, b).

Their main compositional metamorphic foliation (S_1) is subvertical and generally trends NW-SE, although locally it bends to ~ E-W strike defining cm- to dm-scale folds. In the latter places, the superimposition of a second foliation (S_2) is observed, defining very weak crenulation folds (Fig. 3c) with NNE-SSW to NNW-SSE subvertical axial planes. Local stromatitic migmatites (Mehnert 1968) show cm-sized leucosome layers parallel to the asymmetric folds of the S_1 of the meta-

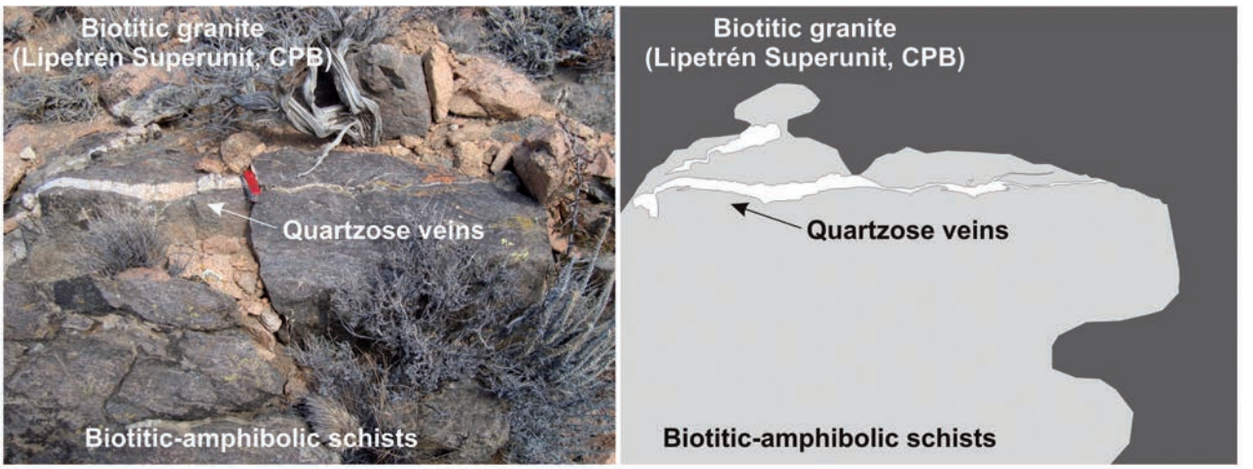

Figure 4: Brittle fracturing and intrusion of quartzose veins in the metamorphic rocks (southern Puesto Rechene area, Fig. 2). Note that the veins do not intrude the biotitic granitoids (Lipetrén Superunit, Central Patagonian Batholith CPB).

morphic rocks (Fig. 3d). The leucosome layers are composed of K-feldspar and quartz and alternate with melanosome layers which are mainly composed of amphibole and biotite.

The metamorphic rocks are intruded by discordant quartz veins which do not intrude the granitoids of the Central Patagonian Batholith. The vein in figure 4 has a very clear, sharp contact with the metamorphic rocks, and appears locally displaced by post-quartz fractures that do not affect the granitoid, pointing thus to a protracted stage of brittle deformation before the intrusion of the granitoids. Individual quartz grains in the vein define a blocky texture.

The schists are composed of quartz, plagioclase, biotite and microcline, accompanied by sillimanite, titanite, apatite and zircon. They have a spaced cleavage defined by the parallel alignment of biotite and quartz (Fig. 5a). The amphibolites are composed mainly of plagioclase, quartz and amphibole, and also have opaque minerals, biotite, titanite, quartz and zircon. They have nematoblastic texture (Fig. 5b). The main foliation S_1 is defined by the general alignment of biotite in the biotitic schists or by hornblende and some minor biotite in the amphibolites. The mineral assemblage seems to have been acquired during greenschist to amphibolite facies conditions.

The local development of the S_2 foliation is hardly seen in thin section because it is less penetrative, but it is suggested by the re-alignment and recrystallization of biotite along the axial planes of the weak folds (Fig. 5b, c). This re-alignment of biotite is what defines the weak crenulation cleavage seen in the outcrop (Fig. 3c), where deformation partitions into high- and low-strain domains (Vernon 2004). Quartz grains are also recrystallized to elongated subgrains which are parallel to the S_2 due to the processes of subgrain rotation and pressure solution that took place during plastic deformation.

Very small, red-coloured euhedral garnet porphyroblasts (typically 2-5 mm across) grew at the expense of the previous metamorphic assemblage without disturbing it (Fig. 5e, f, g). Garnet porphyroblasts seem to appear only in the schists bearing higher biotite/hornblende ratios. They are poikiloblastic, showing inclusions of quartz, plagioclase, biotite and microcline (Fig. 5d, e).

A final retrograde metamorphic event was recognized in the schists given by retrograded sillimanite into muscovite (Fig. 5c, d) and by sericite and chlorite replacing biotite and amphibole.

Granitoids: descriptions in this contribution correspond to rocks which surround the metamorphic rocks and to some neighbor sites located no more than 3 km away from the septum (Figs. 1 and 2). Two different pulses of magmatic rocks are observed, the oldest one is represented by biotite-hornblende granodiorites and subordinate granites belonging to the Gastre Superunit of the Central Patagonian Batholith (Fig. 2, site BTHB-R). The rocks are coarse grained, grey granodiorites with NW-SE, subvertical magmatic foliation defined by the parallelism of biotite, plagioclase, amphibole and elongated mafic microgranular enclaves (Fig. 6a). The foliation in site BTHB-R (Fig. 2) becomes more intense close to the contact with the septums of the metamorphic rocks. These granodiorites experienced deformation at high-temperature conditions, as suggested by the presence of chessboard texture in quartz, the inversion of orthoclase to microcline, and the development of myrmekites.

The biotitic granites of the Lipetrén Superunit (Figs. 1 and 2) intrude the biotite and hornblende granodiorites of the Gastre Superunit. These younger intrusives lack mafic microgranular enclaves and are fine- to locally coarse-grained syeno- to monzogranites. The Lipetrén Superunit granites have clear intrusive contacts with the host rocks, and can be neatly traced in the area (Fig. 2). Several short and narrow (meter- and centimeter- scale, respectively) intra-unit mylonite strips (Fig. 6b, c) suggest that some low-temperature,

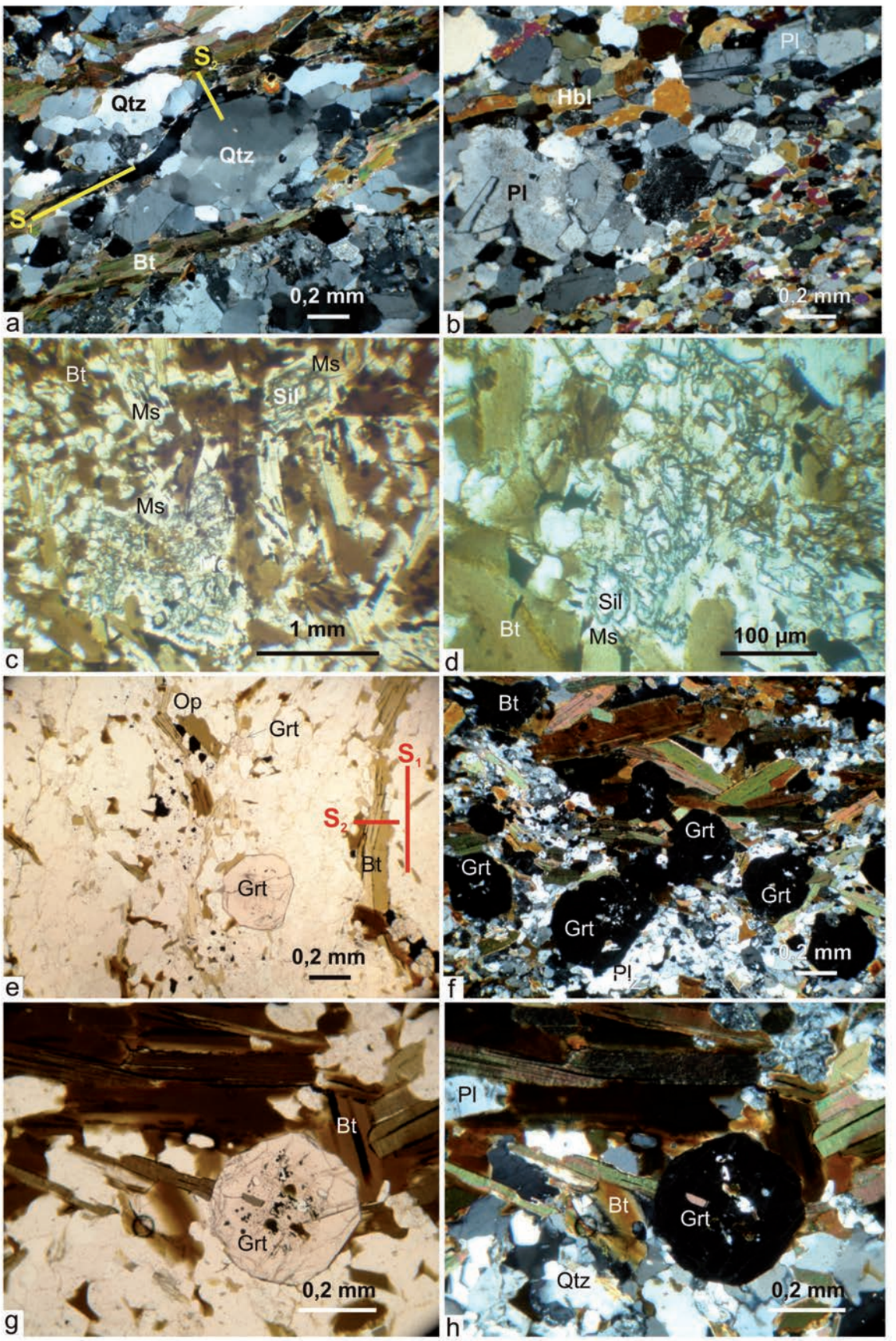

Figure 5: Metamorphic rocks from southern Puesto Rechene area (Fig. 2) in thin section; the slides belong to horizontal surfaces perpendicular to the subvertical foliation planes a) Biotitic schist with spaced cleavage. Biotite crystals are slightly bent defining crenulation folds b) Nematoblastic texture in amphibolite. c) and d) Sillimanite retrograded to muscovite e) Schist with biotitic bands of E-W subvertical orientation (S1 orientation) slightly crenulated defining weak folds and S2 axial surfaces (NW-SE subvertical orientation). Garnet porphyroblasts unevenly scattered throughout the rock. f) Poikiloblastic garnet porphyroblasts with inclusions of biotite, quartz and plagioclase from the matrix. g) Detail of biotite, opaque minerals and quartz inclusions in garnet. h) idem "g", under crossed polars Sil: Sillimanite, Grt: garnet, Pl: plagioclase, Op: opaque minerals, Ms: muscovite, Qtz: quartz, Bt: biotite, Hbl: hornblende.

simple shear deformation took place at the boundaries between adjacent blocks of the pluton.

The biotitic granites show the evidence of deformation during the transition from magmatic to solid-state flow. These fabrics were acquired during the emplacement and cooling process of the magma, and have NW-SE subvertical orientation. Magmatic flow is evidenced by the parallelism of the euhedral and undeformed plagioclase crystals. The superimposition of a high-temperature solid-state recrystallization process is recognized by the inversion of orthoclase to microcline (Fig. 6e), the lobate or irregular margins of quartz and feldspars due to high-temperature grain-boundary migration recrystallization (Vernon 2004; Fig. 6e, f), the chessboard texture present in quartz, and the presence of myrmekites (Fig. 6f). Local shear zones are developed on these granites, where low-temperature solid-state recrystallization is attested by the presence of small quartz and feldspar subgrains formed by bulging recrystallization. The ductile foliation planes are defined by recrystallized quartz and biotite aggregates. In these local shear zones a subvertical lineation defined by the alignment of quartz and biotite crystals was clearly observed.

Slight fracturing of the feldspars and the presence of fine-grained phyllosilicates that define C-type shear bands (Passchier and Trouw 2005) affect the biotitic granites in sites LIPR-M2, LIPR-M3 and LIPR-M4 (Fig. 2). This low-temperature solid-state deformation process generates a superimposed NW-SE subvertical foliation and a subvertical lineation (Fig. 6c). Fine-grained dikes intruding the biotitic granitoids appear sinistrally displaced in site LIPR-M4 as a consequence of this final deformation process (Fig. 6d).

Figure 6: Granitoids from southern Puesto Rechene area (Fig. 2). a) Biotite and hornblende granodiorites from the Gastre Superunit with magmatic foliation of NW-SE subvertical orientation with solid-state deformation superimposed (site BTHB-R, Fig. 2). b) Biotite granites from the Lipetrén Superunit (site LIPR-M1, Fig. 2). The diaclases are parallel to the general NW-SE subvertical trend of the dikes. c) Stretching lineation that rakes 70º from the NE on the NW-SE subvertical foliation plane in site LIPR-M4 (Fig. 2). d) Sinistrally-displaced fine-grained leucocratic dikes intruding the biotitic granites of Lipetrén Superunit in site LIPR-M4. (Fig. 2). e and f) Solid-state deformation in the biotitic granitoids from Lipetrén Superunit in site LIPR-D1.

Puesto Jaramillo locality

In Puesto Jaramillo we observed a ~5 metres wide xenolith of banded muscovitic schists in the biotite and hornblende granodiorites of the Gastre Superunit. The metamorphic compositional folia-

tion of the schists is subvertical and strikes from E-W to NE-SW (Fig. 7a, b). These surfaces are defined by alternating light-coloured bands composed of quartz, plagioclase and microcline and dark bands which are composed of coarse-grained muscovite and opaque minerals (Fig. 7c). The mineral assemblage broadly suggests that the schists reached greenschist to amphibolite facies conditions.

A NW-SE, subvertical foliation is superimposed on the compositional foliation of the schists (Fig. 7a, b). This younger foliation is parallel to the NW-SE, subvertical magmatic foliation observed in the host granitoids (Zaffarana *et al.* 2010). Microstructural observations indicate that this NW-SE subvertical foliation in the host has dominantly developed in magmatic and high-temperature solid-state stages (Zaffarana *et al.* 2010). This suggests that the subvertical folds with NW-SE subvertical axial planes defined in the former compositional surfaces of the muscovitic schists (Fig. 7a) are drag folds resulting from dextral shearing which was likely coeval with the development of the high-temperature solid-state parallel foliation deformation in the host granitoid. Prolonged strain during cooling of plutons must have led to the development of the ~20 cm thick, dextral mylonite strips produced from a granite protolith reported by von Gosen and Loske (2004) for this locality.

ANISOTROPY OF THE MAGNETIC SUSCEPTIBILITY

Anisotropy of the magnetic susceptibility (AMS) measurements have been performed in order to further explore the internal structure of the studied rocks. AMS is a widely accepted technique and a number of studies have investigated the relationship between AMS and strain ellipsoids (e.g. Borradaile and Mothershill 1984, Rochette *et al.* 1992, Hrouda 1993, Borradaile and Henry 1997). AMS is today a standard technique for petrofabric studies in granitoids (e.g. Archanjo *et al.* 1995, Borradaile and Jackson 2010 and references therein), having outstanding relevance in determination of magmatic lineations, which are usually hard to measure in the field as well as in the laboratory using the microscope.

The basic information is the bulk magnetic susceptibility (K_m) of the sample, which is a scalar parameter with compositional significance. The spatial variation of K_m determines the AMS ellipsoid which is represented by its three principal axes (K1≥K2≥K3). These define a magnetic lineation (K1) and a magnetic foliation (plane containing K1 and K2, with K3 being the pole to foliation). Other scalar information used in this paper comprises the Jelinek's mean anisotropy degree (P_J) and the shape parameter (T). P_J varies from 1 for isotropic material to higher values representing increasing anisotropy (i.e. 1.35 = 35% anisotropy). T varies from 1 for perfectly oblate ellipsoid (K1=K2) to -1 for perfectly prolate ellipsoid (K2=K3). The common relationship between the AMS ellipsoid and petrofabric shows the magnetic lineation parallel to the structural lineation (stretching or flow) and the magnetic foliation parallel to the structural foliation (flattening or flow).

This study reports AMS results from 7 sites (Table 1, Appendix), each of them comprising several samples from a certain outcrop of a certain lithology. Two sites belong to Puesto Jaramillo (site MET-J is further divided in the subsites MET-J1 and MET-J2, see Table 1 in the Appendix) and five belong to south of Puesto Rechene area. Whenever possible, foliation plane attitudes were determined in the field in order to compare with the magnetic fabric. AMS measurements on 74 cylindrical specimens were performed by using a MFK1-B Kappabridge susceptibilimeter. AMS susceptibility ellipsoids (with principal axes K1>K2>K3) were calculated from a minimum of five specimens per site using matrix averaging routines (Jelinek 1978) with the programs ANISOFT 4.2 (Chadima and Jelinek 2009; www.agico.com).

South of Puesto Rechene area

Site MET-R out of five sites from south of Puesto Rechene area belongs to the metamorphic rocks in the sector of folded rocks bearing the two foliations S_1 and S_2 (as in Fig. 3, see the previous section). The remaining four sites belong to the biotitic granites of the Lipetrén Superunit, two of them around the metamorphic outcrops (sites LIPR-D1 and LIPR-M1). Site LIPR-D1 represents a ductile shear zone after granite, whereas site LIPR-M1 belongs to granites with magmatic fabric. The other two AMS sites (LIPR-M3 and LIPR-M4) belong to biotitic granites of the Lipetrén Superunit bearing magmatic fabric located nearby (Fig. 2).

The sampled metamorphic rocks have variable bulk magnetic susceptibility (K_m) defining two modes around two different mean values of 0.78×10^{-03} SI and 9×10^{-03} SI (Fig. 8a). Mean bulk susceptibility from the ductilely deformed biotitic granites of the Lipetrén Superunit is 8.17×10^{-03} SI. In the Km versus Jelinek's mean anisotropy degree (P_J) diagram (Fig. 8a), the metamorphic rock samples with higher K_m show a higher P_J, suggesting that the magnetite content may be influencing the parameter of fabric intensity "P_J" (Archanjo *et al.* 1995, Gregoire *et al.* 1995, 1998). A weak direct relationship of P_J with K_m is present in the granites with magmatic fabric (sites LIPR-M1, LIPR-M2 and LIPR-M3), pointing to the amount of magnetite governing the P_J values. In contrast, the rather uniform and high degree of magnetic anisotropy observed in the granites with ductile deformation (35%, from P_J=1.35) suggests that there is a tectonic overprint on the original magnetic fabric associated to magmatic flow.

The shape parameter (T) from all the sites is greater than zero, reflecting that at site level there is a good development of the magnetic foliation, in agreement with the dominance of planar fabrics observed in outcrops (Fig. 8b). The individual samples from the sites have positive T parameters, with the exception of some

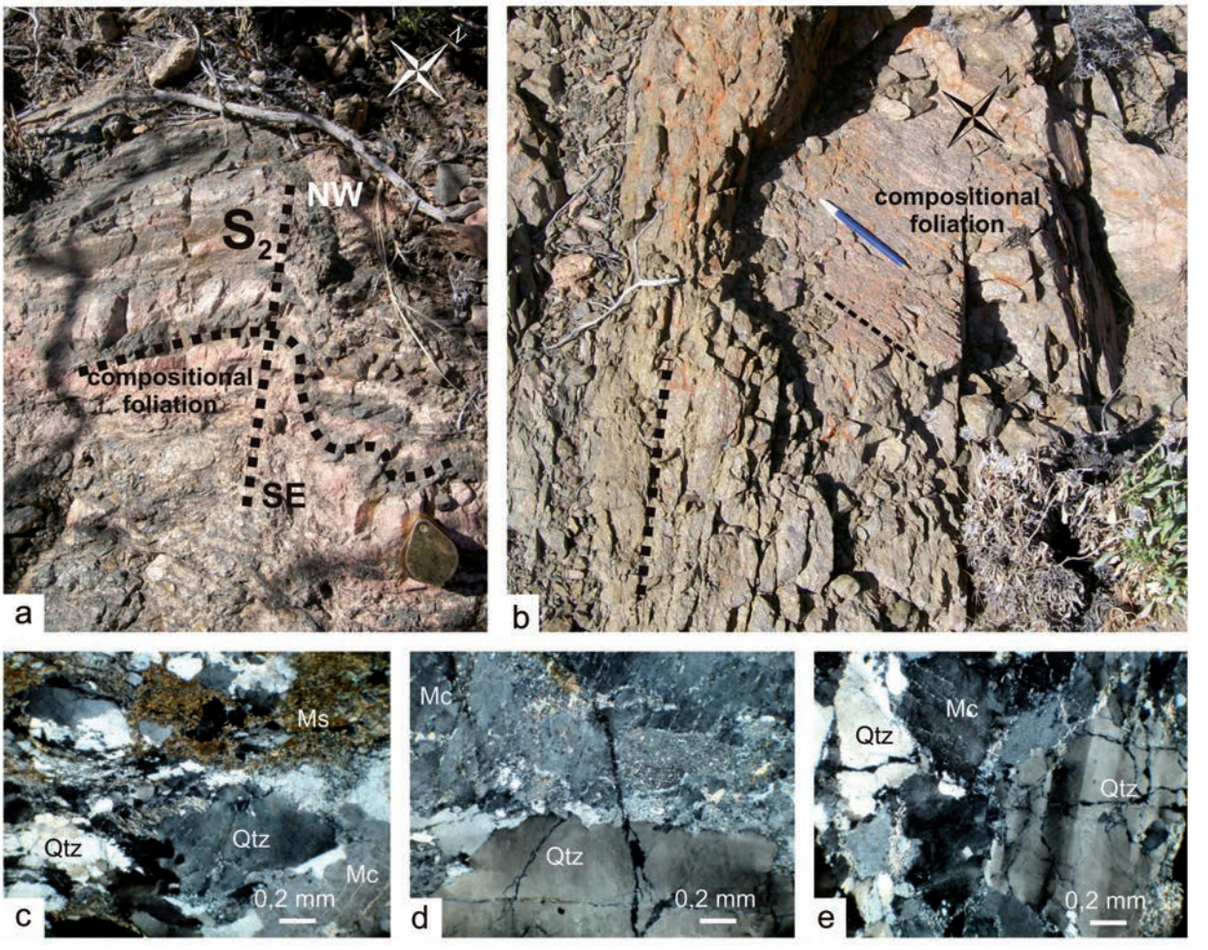

Figure 7: Banded muscovitic schists from Puesto Jaramillo (Fig. 1) a) Plan view of a dextral drag fold with subvertical NW-SE axial planes. b) Plan view of the muscovitic schists having S1 foliation planes with E-W subvertical orientation and superimposed S2 foliation planes of NW-SE subvertical orientation. c) Thin section of the muscovitic schists showing a banded structure with lepidoblastic muscovitic domains and microlithons with quartz, plagioclase and microcline. d) and e) Deformation microstructures in the schists: quartz and microcline porphyroclasts with undulose to fragmentose extinction surrounded by aggregates of dynamically recrystallized quartz and foliated aggregates of neocrystallized micas.

samples from the biotitic granites with magmatic fabric (sites LIPR-M1, LIPR-M2 and LIPR-M3), whose T parameter is negative or close to zero (Fig. 8b). As is discussed in the following paragraphs, the visual inspection of the obtained anisotropy stereograms reveals that their shape is triaxial in all the sites, so a direction of magnetic lineation can be obtained from them as well.

The tensorial data from the metamorphic rocks tend to reflect two slightly different magnetic fabrics, one of them for the low-susceptibility samples and the other one for the limited number (n=3) of high-susceptibility samples (Fig. 8c). The low-susceptibility samples (Km < 1 x 10^{-3} SI) belong to the outcrop shown in Fig. 3c and define a triaxial ellipsoid with a WNW-ESE, subvertical magnetic foliation and a moderately NW-plunging magnetic lineation (Fig. 8c). This foliation is close (< 20° apart) to the compositional foliation shown by the S_1 in that outcrop. The S_2 remains unnoticed by AMS data. On the other hand, the three high-susceptibility samples (Km ~ 10 x 10^{-3} SI) belong to rocks showing the NW-SE-trending S_1 that characterizes the septum, and the samples define a NW-SE subvertical magnetic foliation which is concordant with the magnetic foliation shown in the granitoids bearing both magmatic and tectonic fabric. Some weak contribution of this high- susceptibility ellipsoid could be responsible for the very small clockwise rotation with respect to field data that shows the magnetic anisotropy ellipsoid of the set of low-susceptibility samples. The magnetic lineation from the high-susceptibility samples is not well defined, probably because of the small number (n=3) of samples.

The ductilely deformed biotitic granites of Lipetrén Superunit yielded a NNW-SSE, subvertical magnetic foliation with steeply NW-dipping magnetic lineation, which is compatible with the observations made in the field. The magnetic foliation is also parallel to the metamorphic S_1 and S_2 foliations described in the me-

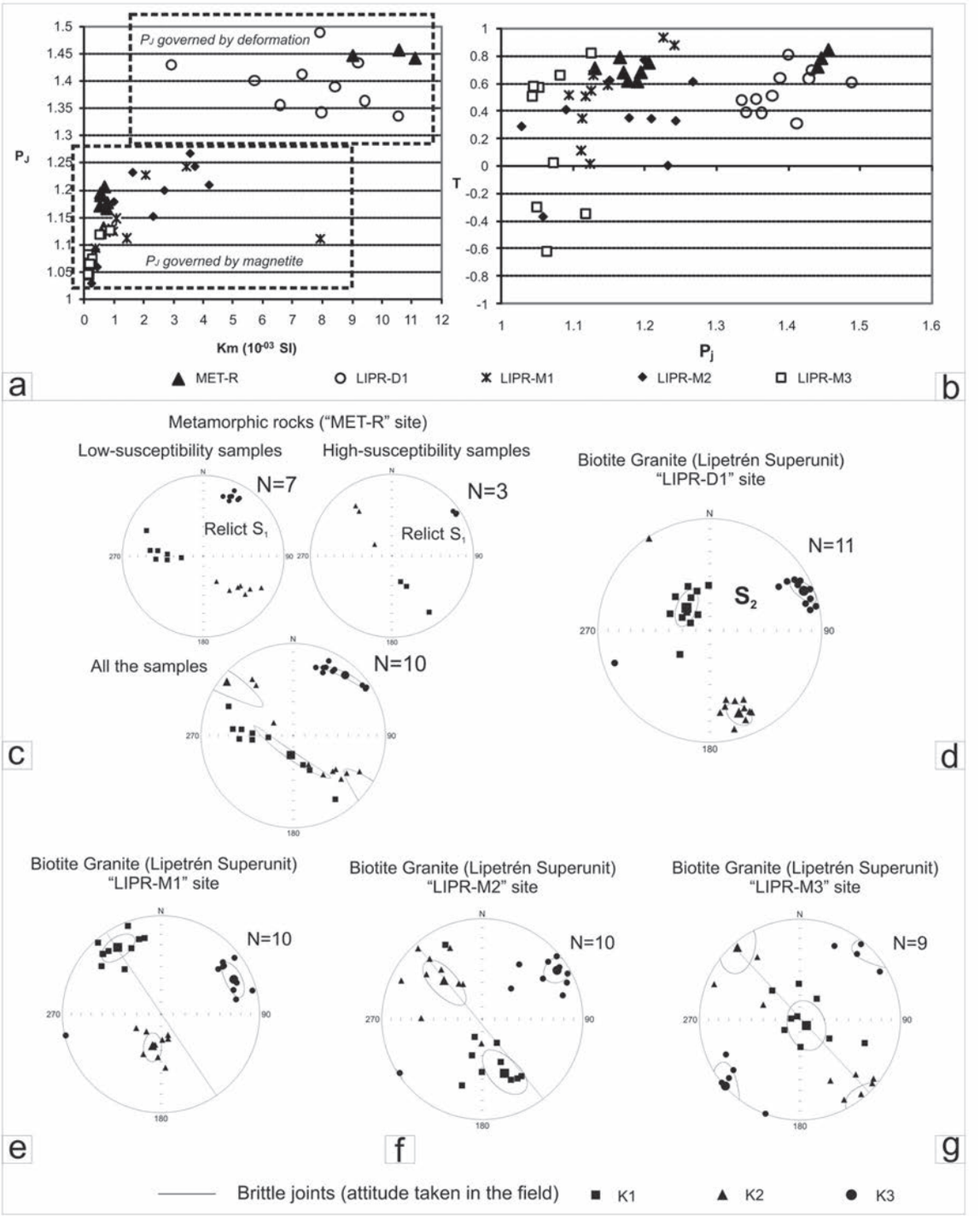

Figure 8: Anisotropy of the magnetic susceptibility from all the sites taken in south of Puesto Rechene area (scalar and vectorial data, anisotropy of the magnetic susceptibility stereograms are lower hemisphere equal area projections). a) Medium susceptibility versus Jelinek's mean anisotropy degree diagram (Km vs. P_J). b) Jelinek's corrected anisotropy degree (P_J) versus shape factor (T) parameter diagram. c) Stereograms of the metamorphic rocks (site MET-R) showing the presence of two fabrics: the samples with lower K define a triaxial ellipsoid with a WNW-ESE, subvertical magnetic foliation and a moderately NW-plunging magnetic lineation, whereas the higher K samples record a NW-SE, subvertical magnetic foliation and have a less defined magnetic lineation. d) Stereogram of the biotitic granites of the Lipetrén Superunit with magmatic to ductile solid-state deformation fabrics in site LIPR-D1 (Fig. 5c). e) Stereogram of the biotitic granites of Lipetrén Superunit in site LIPR-M1; f) Stereogram of the biotitic granites of Lipetrén Superunit in site LIPR-M2. g) Stereogram of the biotitic granites of Lipetrén Superunit in site LIPR-M3. The granites shown in e, f and g have brittle joints superimposed on the magmatic fabric; their orientation was measured in the field and is included on the stereograms.

tamorphic septum.
NW-SE subvertical magnetic foliation planes developed during the magmatic stage were found in the three sites belonging to the biotitic granites of the Lipetrén Superunit (Fig. 8e, f and g). Magnetic lineations are more variable, ranging from subhorizontal in site LIPR-M1 (Fig. 8e), moderately SE-plunging in site LIPR-M2 (Fig. 8f), and subvertical in site LIPR-M3 (Fig. 8g).

Puesto Jaramillo area
The metamorphic rocks from this locality have a low K_m (1.9 x 10^{-4} SI), suggesting that paramagnetic minerals would strongly influence the magnetic anisotropy of the rock. The lack of correlation between bulk magnetic susceptibility and the intensity of the magnetic fabric (P_J vs. Km diagram, Fig. 9a) suggests that P_J may reflect fabric strength. The granitoids of this locality have a much higher K_m (21 x 10^{-03} SI) dominated by multidomain magnetite (Zaffarana *et al.* 2010). The positive correlation observed in the P_J vs. K_m diagram (Fig. 9b) strongly suggests that in these samples P_J depends on the amount of magnetite.
The magnetic fabric of the hosting biotite and hornblende granodiorites from the Gastre Superunit (BTHB-J site) is characterized by NW-SE, subvertical foliation and horizontal lineation (Fig. 9e). Samples from the embedded xenolith (MET-J site) define two magnetic ellipsoids, both showing the same magnetic foliation than the observed in the granitoids (compare the pole to the magnetic foliation -K3- position in Fig. 9d vs. e), implying that the magnetic signal of the compositional foliation of the xenolith was mostly overprinted by a new magnetic foliation acquired when the magmatic fabric of the host granitoid froze. In contrast, two records of the magnetic lineation are observed here. A group of samples (subsite MET-J1, Fig. 9f) shows a subvertical lineation that we interpret as defined by the interception of the observed magnetic foliation and a weak relic of the compositional metamorphic foliation of the xenolith. On the other hand, four samples (subsite MET-J2, Fig. 9g) show a subhorizontal magnetic lineation that would be coeval with the observed magnetic lineation in the host granitoid (Fig. 9e).

GARNET CHARACTERIZATION AND ZONATION PATTERN

A rather peculiar characteristic of the outcrops that we describe is the presence of garnet porphyroblasts in the Cushamen Formation. We have performed eight profiles of chemical analyzes from core to rim along several of these crystals in order to have a better insight about their origin. It is widely acknowledged that garnets show a cryptic zonation due to the variation in contents of MnO, FeO, CaO and MgO as a consequence of the crystal growth process (Hollister 1966, Edmunds and Atherton 1971, Lopez Ruiz and García Cacho 1974, Tuccillo *et al.* 1990). For example, igneous and metamorphic garnets show a decrease in the content of MnO and CaO and an increase in FeO and MgO towards the edge of the crystal (Atherton and Edmunds 1966, Edmunds and Atherton 1971). The resulting bell-shaped zonation curves are due to continuous growth during one metamorphic event. In contrast, garnets that have undergone retrogressive metamorphism show an inverse zonation; where MnO concentration is relatively higher at the margins than in the center of the crystals (Grant and Weiben 1971, Amit 1976). Zonation curves corresponding to garnets originated by contact metamorphism show complex symmetrical or non-symmetrical forms which are due to the non-continuous nature of growth resulting from polyphase metamorphism, and MnO and FeO tend to increase together as a result of thermal growth (Edmunds and Atherton 1971).
Two samples of the metasedimentary rocks of the south of Puesto Rechene area (Fig. 1, Fig. 2) were selected for the garnet zonation studies. Chemical analyses were performed in the Centro de Microscopías Avanzadas (CMA), Facultad de Ciencias Exactas y Naturales, Universidad de Buenos Aires (FCEN-UBA), using an Energy Dispersive X-Ray Microanalysis Hardware (EDS), Inca Energy, Oxford Instruments, coupled to a SEM Zeiss Supra 40 scanning electron microscope equipped with a field emission gun. The images were taken with in-lens detector and 5 kV acceleration voltage. The applied standards were $CaCO_3$ for C, SiO_2 for O and Si, Al_2O_3 for Al, wollastonite for Ca, MgF2 for F and MgO for Mg. Another profile was carried out in CITEFA (Laboratorio de Investigaciones Técnicas de las Fuerzas Armadas), using an Energy Dispersive X-Ray Microanalysis Hardware (EDS), coupled to a Phillips 9100 scanning electron microscope. The images were taken with in-lens detector and 20 kV acceleration voltage, conventional correction ZAF and TKOFF, 25.0º. A 2 micron electron beam and a counting time of 10 seconds were used. The maximum EDS average error is about 2.6% wt. Metallic elements were used as blank samples. The values obtained from the two microprobes are very similar. The measurements were carried out on different points of the core and the rim of each crystal, and eight zonation profiles were obtained.
Eight profiles were constructed, four of them belong to sample BAS1 (Fig. 10, Table 2 in the Appendix) and the other four belong to sample BAS2 (Fig. 11, Table 3 in the Appendix). The average composition of the cores is $Gro_{10}Alm_{45}Sp_{20}Pyr_{25}$, and the average composition of the rims is $Gro_5Alm_{60}Sp_{20}Pyr_{15}$. Although the composition of the garnets is highly variable, the almandine component is the most important, and almandine is the most common species of garnet in metasedimentary rocks (Deer *et al.* 1997). The garnets of Puesto Rechene area have many fluid inclusions with negative crystal morphology. These cavities also host solid inclusions of octaedric opaque minerals, probably magnetite.
Profiles 1 and 2 from sample BAS 1 we-

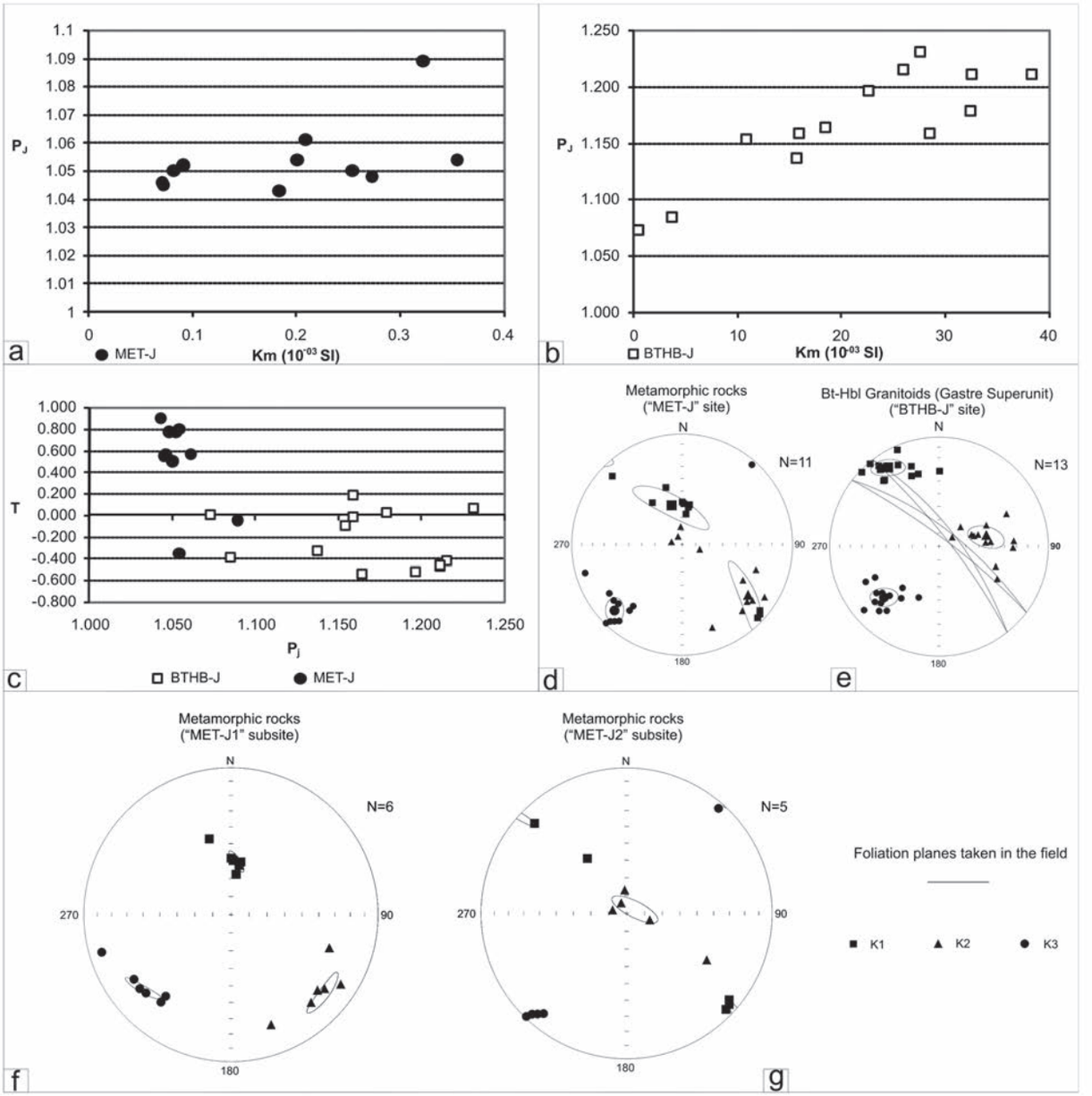

Figure 9: Anisotropy of the magnetic susceptibility of Puesto Jaramillo locality (scalar and vectorial data, anisotropy of the magnetic susceptibility stereograms are lower hemisphere equal area projections). a) Medium susceptibility versus Jelinek's mean anisotropy degree diagram (K_m vs. P_J) for the metamorphic rocks of site MET-J. b) K_m vs. P_J diagram for the biotite and hornblende granitoids, site BTHB-J. c) Jelinek's corrected anisotropy degree (P_J) versus shape factor (T) parameter diagram. d) Stereograms of the metamorphic rocks, site MET-J. e) Stereogram of the intruding biotite and hornblende granitods (site BTHB-J, Gastre Superunit). f) Stereogram of the MET-J1 subsite. g) Stereogram of MET-J2 subsite.

re made on euhedral and unfractured garnet crystals (Fig. 10a, c), whereas garnets from profiles 3 and 4 are euhedral but appear more fractured (Fig. 10e, g). CaO and MgO have a uniform behavior in all the analyzed sections. Profile 1 shows that FeO increases sharply to the rims, whereas MnO is higher in the center than in the rims, although MnO increases slightly next to the rim (Fig. 10b). In profile 2 FeO and MnO tend to vary together defining a very asymmetric pattern, which has a core with peaks and troughs, and where FeO and MnO tend to increase toward the rims (Fig. 10d). In profile 3 (Fig. 10f) FeO and MnO vary together, clearly increasing to the borders. FeO and MnO are not affected by the vicinity of the fracture, suggesting that no diffusion loss has taken place through it. Profile 4 (Fig. 10h) is similar to profile 3, also depicting an increase of FeO and MnO towards the crystal rims. In this case, though, FeO and MnO do

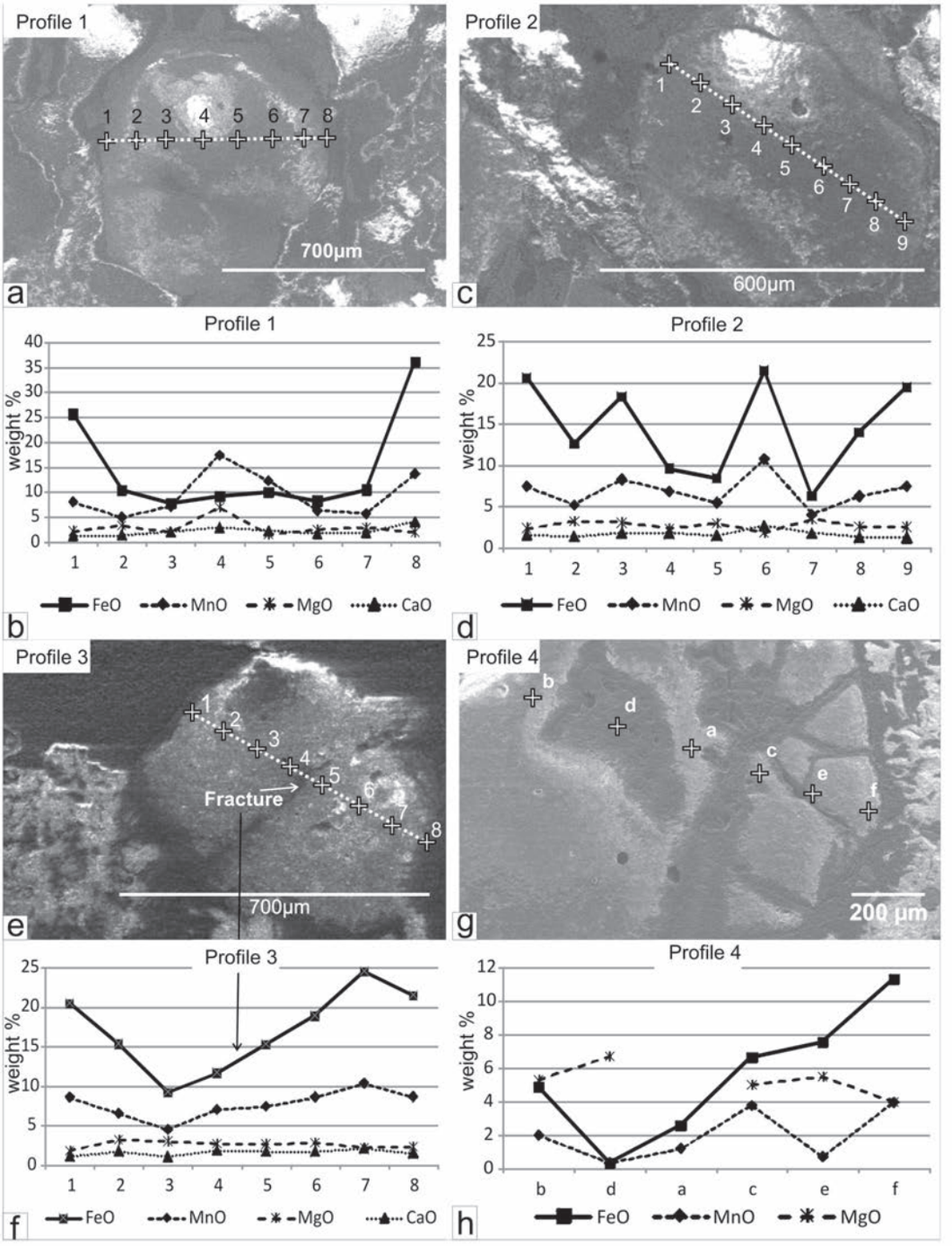

Figure 10: Microphotographs showing the traverses across garnet and chemical analyses of sample BAS1 (biotitic/amphibolic schist).

not vary together as clearly as in profiles 2 and 3.

Profiles 1 and 2 from sample BAS 2 were made on slightly fractured crystals (Fig. 11a, c), and profiles 3 and 4 belong to small, sharp-edged and unfractured crystals (Fig. 11e, g). As in sample BAS1, CaO and MgO show a uniform behavior and FeO and MnO vary together. In profile 1 (Fig. 11b) FeO and MnO increase towards one of the rims. FeO and MnO show an irregular distribution in profile 2 (Fig. 11d) and in profile 4 (Fig. 11h). One of the points of profile 3, located next to a fracture (point 2, Fig. 11f), has a very high FeO and MnO content, suggesting that some diffusion may have taken place through it.

DISCUSSION

Origin of the garnet porphyroblasts

The general zonation pattern of the analyzed garnets is highly asymmetrical, with a

tendency of FeO and MnO to increase together to the rims. With the exception of the center of the garnet analyzed in profile 1 from sample BAS1 (Fig. 10b), the typical bell-shaped zonation pattern produced by regional metamorphism, where MnO and FeO vary in a complementary manner, has not been found here. The increase of MnO and FeO together may be due to an unusually low CaO concentration available in the protolith.

The analyzed garnets from the schist of southern Puesto Rechene area are of small size, and grew without disturbing the previous schistosity, enclosing many quartz, plagioclase, opaque minerals and biotite crystals from the foliated matrix (Fig. 5e-h). All these observations suggest that garnet developed under a fast growth rate, which is typical of contact metamorphism. Besides, garnet porphyroblasts do not appear in all the schists, but only in the biotitic ones, and neither do they appear in the schists from Puesto Jaramillo area located nearby. This fact also suggests that garnet formed as a result of a local process (as the heat input from the intrusions) and not as a result of a regional process.

Some authors have discovered that FeO and MnO increase towards the rims of garnets which have undergone retrograde metamorphism (Grant and Weiblen 1971, Amit 1976), and thus this pattern is not seen exclusively in the rims of garnets formed by thermal metamorphism. Garnets formed by regional followed by retrograde metamorphism are usually cracked, resorbed and have many embayments which are filled with chlorite or muscovite (Amit 1976, Wheeler *et al.* 2004). Another characteristic of garnets affected by retrogression is that MnO is rich near the cracks in the crystal and depleted as the distance from the cracks increases (Amit 1976). The garnets from southern Puesto Rechene area show euhedral shapes, and no resorption has been observed. Even though the schists have endured some retrogression given by the replacement of sillimanite by muscovite and by the presence of chlorite, these minerals are not found in the vicinity of the analyzed garnets. Except by one example (Fig. 11e, f), no increase of FeO and MnO towards the crystal´s cracks was observed. We favor the hypothesis that the highly asymmetrical FeO and MnO zonation with a slight increase to the rims which characterizes these garnets is due to their origin through fast crystallization during thermal metamorphism. Local diffusion along some of the cracks could have taken place as a result of superimposed retrograde metamorphism.

The high Si and Fe content of the garnets (Tables 2 and 3, Appendix) could also be explained by the occurrence of strong metasomatism involving the addition of iron and silica (Deer *et al.* 1997). The high silica could have been provided by the granitoids.

As a summary, garnet porphyroblasts overprint the structures in the wall-rock and their asymmetrical FeO and MnO distribution together with their increase towards the crystal rims are typical of contact metamorphism. Thus, they have likely been originated by static processes triggered by the thermal input provided by the intrusion.

Analysis of the deformation in the basement rocks

Textural evidence and hornblende geobarometry indicate that the plutons of the Central Patagonian Batholith were emplaced in shallow crustal levels (Rapela *et al.* 1991, 1992). The internal structure of these plutons is largely dominated by magmatic strain. Low-temperature deformation is represented by sparse, short and thin mylonite strips with non uniform kinematics (von Gosen and Loske 2004, Zaffarana *et al.* 2010).

The biotitic-amphibolic schists and amphibolites of southern Puesto Rechene area (site Met-R, Fig. 1) show a compositional, NW-SE trending and subvertical S_1 foliation which is locally bent forming cm- to dm-sized folds. Locally, the folded areas show a very weak crenulation that alternatively could be wavy surfaces separating microlithons. Small patches of migmatite were locally observed. The S_1 in these biotitic-amphibolic schists and amphibolites was possibly developed at mid- to mid-lower crustal levels at amphibolite facies metamorphism. These rather deep metamorphic rocks were later uplifted up to brittle conditions, where they were fractured and intruded by silica-rich liquids forming the above described veins (Fig. 4), which were further displaced by later fracturing. The latter epizone environmental conditions for the basement probably continued until the intrusion of the high-level granitoids of the Central Patagonian Batholith. The origin of limited anatexis that led to local migmatization is more obscure. It probably occurred at deeper levels, preceding the uplift and intrusion of the quartz veins.

The shallow nature of the plutons, particularly the ambient pressure of ~1 kbar during the intrusion of the subvolcanic Lipetrén Superunit (Rapela *et al.* 1991, 1992), suggests a high-strength rheology for the basement during the intrusive stage. This makes it difficult to interpret the development of the crenulations of the compositional foliation in association with the intrusive stage. In fact, this localized, very small-scale folding in the basement could have been produced during progressive deformation in an overall amphibolite-facies environment.

Magmatic fabric in the biotite and hornblende granodiorites from Puesto Jaramillo persistently shows NW-SE subvertical foliation which is in turn parallel to the magnetic foliation detected in these rocks (Zaffarana *et al.* 2010), strongly suggesting that the associated, subhorizontal magnetic lineation (Zaffarana *et al.* 2010) is coincident with the elongation of the magmatic strain ellipsoid. The xenolith of Cushamen Formation at Puesto Jaramillo shows a distinct, E-W compositional foliation (Fig. 7a, b) and a superimposed NW-SE foliation (Fig. 7b) that i) is parallel to the foliation in the hosting granodiorites and ii) locally displaces the compositional foliation in the xenolith

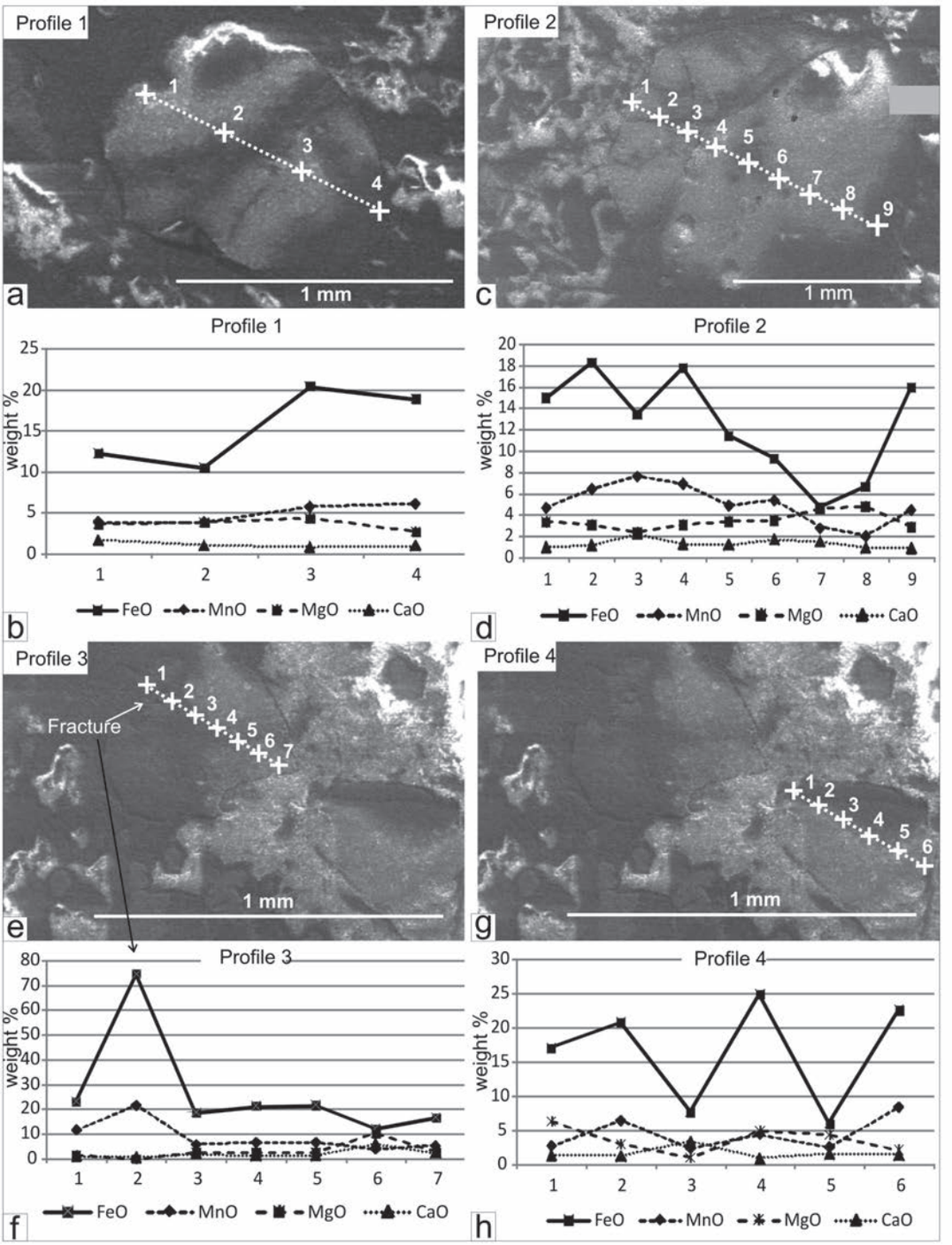

Figure 11: Microphotographs showing the traverses across garnet and chemical analyses of sample BAS 2 (biotitic/amphibolic schist).

forming dextral drag folds (Fig. 7a). The latter solid-state deformation could have developed in high- and/or in low-temperature conditions. If this deformation was coeval with the high-temperature solid-state deformation in the granodiorite host described above in Section 3.1, it occurred mostly under high-temperature conditions, but if it was coeval with the development of dextral mylonite strips found by von Gosen and Loske (2004) in this locality and with the solid-state transposition of the magnetic fabric in mafic dikes reported by Zaffarana *et al.* (2010) also in this locality, then it occurred in low-temperature conditions. Likewise, the two magnetic lineations observed in the xenolith record deformation that postdates the magmatic state of the granodiorite host. The subvertical magnetic lineation is likely reflecting the intersec-

tion of the two xenolith foliations observed in the field (NW-SE and E-W, Fig. 7a, see above). The subhorizontal magnetic lineation likely corresponds to that observed by AMS in the granitoids. Thus, AMS in this locality allows us to attribute the post-intrusion (i.e. Late Triassic until perhaps earliest Jurassic) solid-state deformation observed in the xenolith, dikes and mylonite strips to the consolidation and cooling history of the granodiorites.

CONSIDERATIONS ABOUT THE "SO-CALLED" GASTRE FAULT SYSTEM

Newly found outcrops of the host rock of the Central Patagonian Batholith (CPB) in Gastre form an association of micashcists, amphibolites and metaquartzites with local migmatization that resembles the general appearance of the Cushamen Formation reported in other localities (e.g. Dalla Salda *et al.* 1994). This allows the assertion that the plutons that compose the Central Patagonian Batholith intruded a pre-Triassic geology formed by at least three units: the Cushamen, the Calcatapul and the Mamil Choique formations. The observed outcrops of the Cushamen Formation at Gastre correspond to biotitic-amphibolic schists and to amphibolites that suggest greenschist to amphibolite facies metamorphism. Garnet is observed as a late product of contact metamorphism.

The internal structure of the plutonic rocks that enclose the Cushamen Formation outcrops is largely the product of magmatic flow with NW-SE subvertical foliation and variable lineation. Low-temperature, solid-state deformation in the Gastre region (Fig. 1) is represented by only very small strips with no regional kinematics significance (Zaffarana 2011). For instance, the sinistral and almost dip-slip, low-temperature deformation in the granitoids from the south of Puesto Rechene area (Fig. 6c, d) contrast with the dominant dextral strike-slip deformation that is dominant in Puesto Jaramillo (Fig. 7a, see also von Gosen and Loske 2004), as well as with the top-to-the-east reversed mylonites found near the village of Gastre (von Gosen and Loske 2004), and with the dip-slip and sinistral shearing observed at Estancia Yancamil (von Gosen and Loske 2004, Zaffarana *et al.* 2010). Altogether, the integrated structural data point to a picture of heterogeneous deformation in the Gastre region, which is possibly related to local accommodations related to the successive emplacement of multiple magma batches that in amalgamation composed the Central Patagonian Batholith (e.g. Coleman *et al.* 2004). This heterogeneous deformation strongly diminishes the rather homogeneous deformation required by the hypothesis of a Gastre Fault System as a large, transcontinental dextral shear zone passing across the studied area (e.g. Marshall *et al.* 1994, Martin *et al.* 2007 and references therein).

AKNOWLEDGEMENTS

This work was partially supported by PIP 02828 and UBACyT X200. C.B.Z. acknowledges Dra. Mónica López de Luchi for her early guidance in petrographic analyzes. An early version of the manuscript was improved by comments from two anonymous reviewers.

APENDIX

TABLE 1: Anisotropy of the magnetic susceptibility (AMS) results.

Site	Lithology	Fabric	N	Km (E^{-03} SI)	St Dev (E^{-03} SI)	F	L	Pj	T						
Puesto Jaramillo															
BTHBL-J	Bt-Hbl Gr (Gastre Superunit)	Magmatic + Subsolidus	13	21	11.4	1.09	1.057	1.153	-0.215	1076	0,938	326,7	12	230,1	28,5
MET-J	Metamorphic rocks (all samples)	Metamorphic S1 + S2	11	0.192	0.103	1.007	1.037	1.048	0.656	1.017	0.974	345	59.9	225.8	15.7
MET-J1 subsite	Metamorphic rocks (6/11 samples)	Metamorphic S1 + S2	6	0.166	0.135	1.02	1.032	1.053	0.228	1.023	0.973	5.7	60.3	229.1	22.5
MET-J2 subsite	Metamorphic rocks (5/11 samples)	Solid state S2	5	0.224	0.0377	1.007	1.04	1.05	0.709	1.017	0.972	312.3	2.1	222.1	4.7
South of Puesto Rechene area															
MET-R	Metamorphic rocks	Metamorphic S1 + S2	10	3.53	4.66	1.016	1.174	1.215	0.818	1.063	0.891	187	72.6	40.6	14.6
LIPR-D1	Bt Gr (Lipetrén Superunit)	Magmatic + Subsolidus	11	8.17	2.76	1.063	1.258	1.358	0.582	1.116	0.835	314.2	66.3	67.1	9.7
LIPR-M1	Bt Gr (Lipetrén Superunit)	Magmatic	10	1.96	2.28	1.024	1.093	1.126	0.586	1.045	0.934	327	20.3	64.5	19.2
LIPR-M2	Bt Gr (Lipetrén Superunit)	Magmatic	10	2.02	1.49	1.032	1.098	1.139	0.5	1.052	0.928	157.8	41.4	56.8	12.2
LIPR-M3	Bt Gr (Lipetrén Superunit)	Magmatic	9	0.287	0.246	1.021	1.035	1.057	0.244	1.057	0.97	132.5	82.9	228.3	0.7

Km (St.Dev) is mean magnetic susceptibility (standard deviation), L is mean lineation, F is mean foliation, P' is corrected anisotropy degree (Jelinek 1981), T is shape parameter (Jelinek 1981) where $0 < T < 1$ indicates oblateness and $1 < T < 0$ indicates prolateness, Dec and Inc are declination and inclination of downward direction. Bt-Hbl Gr: biotite - hornblende granodiorites, Bt Gr: biotitic granites.

TABLE 2: Garnet analyses of sample BAS 1 (biotitic/amphibolic schist).

Sample	BAS1 - Profile 1								Sample J13 - Profile 2								
Oxides wt%)	1	2	3	4	5	6	7	8	1	2	3	4	5	6	7	8	9
SiO_2	36.99	50.31	50.49	40.71	46.85	52.30	53.33	31.04	42.94	50.31	43.83	48.08	51.84	41.29	53.37	48.54	44.33
Al_2O_3	25.53	29.32	30.48	22.43	26.88	28.70	25.41	12.87	25.03	27.16	24.73	31.23	29.69	21.95	30.99	27.33	25.02
FeO	25.78	10.56	7.92	9.31	10.15	8.38	10.63	36.18	20.63	12.71	18.35	9.69	8.51	21.52	6.34	14.03	19.48
MnO	8.05	4.92	7.08	17.49	12.26	6.26	5.66	13.71	7..47	5.23	8.29	6.87	5.52	10.75	4.07	6.31	7.47
MgO	2.27	3.43	1.91	7.06	1.59	2.59	2.99	2.06	2.36	3.23	3.01	2.35	2.96	1.81	3.43	2.52	2.50
CaO	1.38	1.46	2.13	3.00	2.27	1.76	1.98	4.13	1.57	1.36	1.79	1.79	1.48	2.67	1.79	1.27	1.20
Total	100	100	100	100	100	100	100	100	100	100	100	100	100	100	100	100	100
Element (moles)																	
Si	5.83	7.01	7.02	6.21	6.82	7.24	7.85	5.55	6.48	7.10	6.57	7.10	7.15	6.43	7.22	6.95	6.63
Al	4.74	4.82	5.00	4.03	4.61	4.68	4.41	2.71	4.46	4.52	4.37	5.43	4.83	4.03	4.94	4.61	4.41
Mn	1.07	0.58	0.83	2.26	1.51	0.73	l0.71	2.08	0.96	0.63	1.05	0.86	0.65	1.42	0.47	0.76	0.95
Mg	0.53	0.71	0.40	1.60	0.34	0.53	0.66	0.55	0.53	0.68	0.67	0.52	0.61	0.42	0.69	0.54	0.56
Ca	0.23	0.22	0.32	0.49	0.35	0.26	0.31	0.79	0.25	0.21	0.29	0.28	0.22	0.45	0.26	0.19	0.19
Fe	3.40	1.23	0.92	1.19	1.24	0.97	1.31	5.41	2.61	1.50	2.30	1.20	0.98	2.80	.072	1.68	2.44
Components (mol %)																	
Py	10.19	26.01	16.04	28.96	10.01	21.39	22.00	6.23	12.24	22.58	15.59	18.11	24.81	8.27	32.41	16.91	13.48
Alm	64.86	44.85	37.33	21.42	35.86	38.80	43.88	61.28	59.94	49.82	53.35	41.90	39.98	55.10	33.58	52.89	58.97
Gro	4.44	7.96	12.84	8.86	10.27	10.44	10.48	8.97	5.83	6.85	6.67	9.91	8.93	8.75	12.16	6.13	4.66
Sp	20.51	21.18	33.78	40.77	43.86	29.36	23.63	23.52	21.98	20.75	24.39	30.08	26.29	27.87	21.84	24.07	22.89

Sample	Sample BAS1 - Profile 3								Sample BAS1 - Profile 4					
Oxides wt%)	1	2	3	4	5	6	7	8	a	b	c	d	e	f
SiO_2	43.79	46.71	46.21	48.85	47.63	43.77	40.36	43.04	52.25	43.27	49.54	50.36	47.82	46.67
Al_2O_3	24.17	26.32	35.87	27.79	25.22	24.07	20.42	22.95	43.94	44.54	34.99	42.27	38.42	34.03
FeO	20.48	15.39	9.29	11.72	15.29	18.95	24.52	21.47	2.58	4.91	6.65	0.35	7.58	11.33
MnO	8.59	6.55	4.48	7.01	7.44	8.61	10.36	8.63	1.23	2.01	3.82	0.35	0.71	4.00
MgO	1.82	3.21	3.02	2.70	2.64	2.84	2.18	2.36	0.00	5.27	5.00	6.68	5.47	3.97
CaO	1.15	1.81	1.13	1.94	1.78	1.77	2.16	1.55	0.00	0.00	0.00	0.00	0.00	0.00
Total	100	100	100	100	100	100	100	100	100	100	100	100	100	100
Element (moles)														
Si	6.62	6.79	6.41	6.95	6.94	6.59	6.39	6.58	6.76	5.80	6.71	6.50	6.42	6.50
Al	4.31	4.51	5.86	4.66	4.33	4.27	3.81	4.13	6.70	7.04	5.59	6.43	6.08	5.59
Mn	1.10	0.81	0.53	0.84	0.92	1.10	1.39	1.12	0.13	0.23	0.44	0.04	0.08	0.47
Mg	0.41	0.70	0.62	0.57	0.57	0.64	0.51	0.54	0.00	1.05	1.01	1.29	1.10	0.82
Ca	0.19	0.28	0.17	0.30	0.28	0.29	0.37	0.25	0.00	0.00	0.00	0.00	0.00	0.00
Fe	2.59	1.87	1.08	1.39	1.86	2.39	3.25	2.74	0.28	0.55	0.75	0.04	0.85	1.32
Components (mol %)														
Py	9.56	19.04	26.07	18.46	15.77	14.45	9.33	11.54	0.00	57.49	45.86	94.47	54.02	31.53
Alm	60.42	51.17	44.95	44.85	51.29	54.16	58.86	59.01	67.50	30.02	34.21	2.74	42.00	50.45
Gro	4.35	7.73	7.01	9.53	7.67	6.48	6.63	5.44	0.00	0.00	0.00	0.00	0.00	0.00
Sp	25.67	22.07	21.97	27.16	25.27	24.92	25.18	24.01	32.50	12.48	19.92	2.79	3.98	18.02

All Fe was assumed to be Fe^{+2}. Formulae were calculated on the basis of 24 oxygens. Gr= grossular, Py= pyrope, Alm= almandine, Sp= spessartine.

TABLE 3: Garnet analyses of sample BAS 2 (biotitic/amphibolic schist).

	Sample BAS 2 - Profile 1					Sample BAS 2 - Profile 2								
Oxides wt%)	1	2	3	4	5	1	2	3	4	5	6	7	8	9
SiO_2	50.10	50.62	41.50	45.22	47.13	48.85	44.96	46.63	45.35	50.51	51.26	55.67	52.80	47.69
TiO_2	0.00	0.00	1.29	0.00	0.00	0.00	0.00	0.00	0.00	0.00	0.00	0.00	0.00	0.00
Al_2O_3	28.39	29.96	22.56	26.00	26.52	27.15	26.08	27.67	25.60	28.55	28.89	30.62	32.73	28.04
FeO	12.26	10.55	20.42	18.88	1.09	14.99	18.28	13.48	17.76	11.44	9.27	4.77	6.69	16.00
MnO	3.92	3.94	5.76	6.11	5.56	4.69	6.44	7.62	6.92	4.91	5.38	2.81	2.05	4.50
MgO	3.59	3.82	4.33	2.74	2.76	3.35	3.08	2.38	3.09	3.38	3.51	4.59	4.80	2.90
K_2O	1.74	1.11	0.88	1.06	16.95	0.98	1.17	2.22	1.27	1.21	1.69	1.54	0.94	0.87
CaO	0.00	0.00	3.27	0.00	0.00	0.00	0.00	0.00	0.00	0.00	0.00	0.00	0.00	0.00
Total	100	100	100	100	100	100	100	100	100	100	100	100	100	100
Element (moles)														
Si	7.02	7.01	6.37	6.67	6.84	6.97	6.64	6.75	6.69	7.07	7.11	7.41	7.08	6.84
Al	4.69	4.89	4.08	4.52	4.54	4.56	4.54	4.72	4.45	4.71	4.73	4.80	5.17	4.74
Ti	0.00	0.00	0.15	0.76	0.68	0.00	0.00	0.00	0.00	0.00	0.00	0.00	0.00	0.00
Mn	0.47	0.46	0.75	0.60	0.60	0.57	0.80	0.93	0.87	0.58	0.63	0.32	0.23	0.55
Mg	0.75	0.79	0.99	0.17	2.06	0.71	0.68	0.51	0.68	0.71	0.73	0.91	0.96	0.62
Ca	0.26	0.16	0.14	2.33	0.17	0.15	0.18	0.34	0.20	0.18	0.25	0.22	0.13	0.13
Fe^{+2}	1.44	1.22	2.62	0.00	0.00	1.79	2.26	1.63	2.19	1.34	1.08	0.53	0.75	1.92
K	0.00	0.00	0.64	0.00	0.00	0.00	0.00	0.00	0.00	0.00	0.00	0.00	0.00	0.00
Components (mol %)														
Py	25.74	29.92	21.99	5.38	72.87	22.13	17.29	15.01	17.29	25.13	27.01	46.04	46.23	19.27
Alm	49.33	46.34	58.19	0.00	0.00	55.61	57.51	47.65	55.65	47.69	40.06	26.84	36.11	59.61
Gro	8.94	6.22	3.20	75.19	6.02	4.64	4.70	10.07	5.09	6.44	9.38	11.11	6.47	4.16
Sp	15.99	17.52	16.62	19.42	21.12	17.62	20.51	27.27	21.97	20.74	23.55	16.01	11.19	16.96

	Sample BAS 2 - Profile 3							Sample BAS 2 - Profile 4					
Oxides wt%)	3	4	5	6	7	8	9	1	2	3	4	5	6
SiO_2	40.34	1.76	44.74	44.31	43.76	43.64	45.88	35.11	45.48	53.33	38.61	53.90	43.66
TiO_2	0.00	0.00	0.00	0.00	0.00	0.00	0.00	0.00	0.00	0.00	0.00	0.00	0.00
FeO	23.16	74.62	18.71	21.38	21.73	12.30	16.66	17.11	20.81	7.63	24.93	6.01	22.60
Al_2O_3	22.49	1.39	26.18	23.85	23.85	23.85	26.29	17.02	23.00	24.24	21.24	31.60	21.78
MnO	11.67	21.65	5.77	6.60	6.67	3.86	5.30	2.75	6.47	2.39	4.41	2.57	8.41
MgO	1.38	0.00	2.70	2.66	2.70	10.26	3.01	6.26	2.92	1.02	4.84	4.33	2.12
CaO	0.96	0.58	1.90	1.20	1.30	6.09	2.30	1.40	1.30	3.45	0.94	1.60	1.43
Na_2O	0.00	0.00	0.00	0.00	0.00	0.00	0.00	0.00	0.00	7.94	0.00	0.00	0.00
K_2O	0.00	0.00	0.00	0.00	0.00	0.00	0.56	1.34	0.00	0.00	3.98	0.00	0.00
Total	100	100	100	100	100	100	100	100	100	100	100	100	100
Element (moles)													
Si	6.34	0.48	6.61	6.67	6.61	6.78	6.72	6.55	6.81	7.49	6.11	7.23	6.69
Al	4.16	0.45	4.56	4.23	4.25	4.37	4.54	3.74	4.06	4.01	3.96	4.99	3.94
Ti	0.00	0.00	0.00	0.00	0.00	0.00	0.00	0.00	0.00	0.00	0.12	0.00	0.00
Mn	1.55	5.04	0.72	0.84	0.85	0.51	0.66	0.43	0.82	0.28	0.59	0.29	1.09
Mg	0.32	0.00	060	0.60	0.61	2.38	066	1.74	0.65	0.21	1.14	0.86	0.48
Ca	0.16	0.17	0.30	0.19	0.21	1.01	0.36	0.28	0.21	0.52	0.16	0.23	0.24
Fe^{+2}	3.04	17.15	2.31	2.69	2.74	1.60	2.04	2.67	2.61	0.90	3.30	0.67	2.90
K	0.00	0.00	0.00	0.00	0.00	0.00	0.11	0.32	0.00	0.00	0.80	0.00	0.00
Na	0.00	0.00	0.00	0.00	0.00	0.00	0.00	0.00	0.00	2.16	0.00	0.00	0.00
Components (mol %)													
Py	6.38	0.00	15.14	13.82	13.76	43.23	17.70	33.97	15.22	11.19	22.00	41.98	10.27
Alm	59.90	76.71	58.84	62.25	62.17	29.08	54.92	52.11	60.75	46.81	63.55	32.69	61.54
Gro	3.17	0.76	7.65	4.47	4.75	18.44	9.69	5.44	4.91	27.14	3.07	11.16	4.99
Sp	30.55	22.53	18.37	19.46	19.31	9.25	17.68	8.47	19.12	14.85	11.38	14.17	23.20

All Fe was assumed to be Fe^{+2}. Formulae were calculated on the basis of 24 oxygens. Gr= grossular, Py= pyrope, Alm= almandine, Sp= spessartine.

WORKS CITED IN THE TEXT

Amit, O. 1976. Retrograde zoning in garnets from Elat-Wadi Magrish metamorphic rocks. Lithos 9: 259-262.

Archanjo, C.J., Launeau, P. y Bouchez, J.L. 1995. Magnetic fabric vs. magnetite and biotite shape fabrics of the magnetite-bearing granite pluton of Gameleiras (Northeast Brazil). Physics of the Earth and Planetary Interior 89: 63-75.

Archanjo, C.J., Trindade, R.I.F., Bouchez, J.L. y Ernesto, M. 2002. Granite fabrics and regional-scale strain partitioning in the Seridó belt (Borborema Province, NE Brazil). Tectonics 21: 1003.

Atherton, M.P. y Edmunds, W.M. 1966. An election microprobe study of some zoned garnets from metamorphic rocks. Earth and Planetary Science Letters 1: 185-193.

Borradaile, G.J. y Henry, B. 1997. Tectonic applications of magnetic susceptibility and its anisotropy. Earth-Science Reviews 42: 49-93.

Borradaile, G.J. y Jackson, M. 2010. Structural geology, petrofabrics and magnetic fabrics (AMS, AARM, AIRM). Journal of Structural Geology 31: 1519-1551.

Borradaile, G.J. y Mothershill, J.S. 1984. Coaxial deformed and magnetic fabrics without simply correlated magnitudes of principal values. Physics of the Earth and Planetary Interiors 35: 294-300.

Cerredo, M.E. y López de Luchi, M.G. 1998. Mamil Choique Granitoids, southwestern North Patagonian Massif, Argentina: magmatism and metamorphism associated with a polyphasic evolution. Journal of South American Earth Sciences 11: 499-515.

Cerredo, M. E. y López de Luchi, M. G. 1999. Metavolcanics within the metamorphic series of Cushamen Formation. North Patagonian Massif. 14º Congreso Geológico Argentino, Actas 2: 137-139, Buenos Aires.

Coira, B.L., Nullo, F., Proserpio, C. y Ramos, V.A. 1975. Tectónica de basamento en la región occidental del Macizo Norpatagónico (Prov. de Río Negro y Chubut) República Argentina. Revista de la Asociación Geológica Argentina 30: 361-383.

Coleman, D.S., Gray, W. y Glazner, A.F. 2004. Rethinking the emplacement and evolution of zoned plutons: Geochronologic evidence for incremental assembly of the Tuolumne Intrusive Suite, California. Geology 32: 433-436.

Chadima, M. y Jelinek, V. 2009. Anisoft 4.2, Anisotropy data browser for Windows. www.agico.com

Dalla Salda, L., Varela, R., CIngolani, C. y Aragón, E. 1994. The Río Chico Paleozoic Crystalline Complex and the evolution of Northern Patagonia. Journal of South American Earth Sciences 7: 377-386.

Deer, W.A., Howie, R.A. y Zussman, J. 1997. Rock forming minerals: Volume 1A, Orthosilicates. Second Edition, Geological Society of London, 919 p., Oxford.

Duhart, P., Haller, M. y Hervé, F. 2002. Diamictitas como parte del protolito de las metamorfitas de la Formación Cushamen en Río Chico, provincias de Río Negro y Chubut, Argentina. 15º Congreso Geológico Argentino, Actas 2: 97-100, Buenos Aires.

Edmunds, W.M. y Atherton, M.P. 1971. Polymetamorphic evolution of garnet in the Fanad aureole, Donegal, Eire. Lithos 4: 147-161.

Figari, E.F., Courtade, S.F. y Constantini, L.A., 1994. Estratigrafía y tectónica de los bajos de Gastre y Gan Gan. Boletín de Informaciones Petroleras: 40: 75-82.

Franzese, J.R., Pankhurst, R.J., Rapela, C.W., Spalletti, L.A., Fanning, C.M. y Muravchick, M. 2002. Nuevas evidencias geocronológicas sobre el magmatismo gondwánico en el noroeste del Macizo Norpatagónico. 15º Congreso Geologico Argentino, Actas 1: 144-148, Buenos Aires.

Grant, J.A. y Weiblen, P.W. 1971. Retrograde zoning in garnet near the second sillimanite isograd. American Journal of Science 270: 281-296.

Gregoire, V., Darrozes, J., Gaillot, P., Nedelec, A. y Launeau, P. 1998. Magnetite grain shape fabric and distribution anisotropy vs. rock magnetic fabric: A three dimensional case study. Journal of Structural Geology 20: 937-944.

Gregoire, V., de Saint Blanquat, M., Nedelec, A. y Launeau, P. 1995. Shape anisotropy versus magnetic interactions of magnetite grains: Experiments and application to AMS in granitic rocks. Geophysical Research Letters 22: 2765-2768.

Hervé, F., Haller, M.J., Duhart, P. y Fanning, C.M. 2005. SHRIMP U-Pb ages of detrital zircons from Cushamen and Esquel Formations, North Patagonian Massif: Geological Implications. 16º Congreso Geológico Argentino, Actas 1: 309-314.

Hollister, L.S. 1966. Garnet zoning: an interpretation based on the Rayleigh fractionation model. Science 154: 1647-1651.

Hrouda, F. 1993. Theoretical models of magnetic anisotropy to strain relationship revisited. Physics of the Earth and Planetary Interiors 77: 237-249.

Jelinek, V. 1978. Statistical processing of anisotropy of magnetic susceptibility measured in groups of specimens. Studia Geophysica and Geodaetica 22: 50-62.

Linares, E., Cagnoni, M., Do Campo, M. y Ostera, H. 1988. Geochronology of metamorphic and eruptive rocks of southeastern Neuquen and northwestern Río Negro provinces, Argentine Republic. Journal of South American Earth Sciences 1: 53-61.

Linares, E., Haller, M., Ostera, H., Cagnoni, M. y Galante, G. 1997. Radiometric ages of the crystalline basement of the Rio Chico region, Ñorquinco Department, Río Negro Province, Argentina. 1º South American Symposium on Isotope Geology, Extended Abstracts: 170-173, São Paulo.

López de Luchi, M.G. y Cerredo, M.E. 2008. Geochemistry of the Mamil Choique granitoids at Rio Chico, Río Negro, Argentina: Late Paleozoic crustal melting in the North Patagonian Massif. Journal of South American Earth Sciences 25: 526-546.

López de Luchi, M.G., Ostera, H., Cerredo, M.E., Cagnoni, M. y Linares, E. 2000. Permian magmatism in Sierra de Mamil Choique, North Patagonian Massif, Argentina. 9º Congreso Geológico Chileno, Actas 2: 750-754, Santiago.

Lopez Ruiz, J. y García Cacho, L. 1974. The garnets of the eastern area of the Sierra de Guadarrama, Sistema Central, Spain. Chemical Geology 13: 269-283.

Llambías, E.J., Llano, J.A., Rossa, N., Castro, C.E. y Puigdomenech, H.H. 1984. Petrografía de la Formación Mamil Choique en la Sierra del Medio, Departamento de Cushamen-Provincia del Chubut, 9º Congreso Geológico Argentino, Actas 2: 554-567, Buenos Aires.

Marshall, J.E.A., 1994. The Falkland Islands: A key in Gondwana Paleogeography. Tectonics, 13: 499-514.

Martin, A.K., 2007. Gondwana breakup via dou-

ble-saloon-door rifting and seafloor spreading in a backarc basin during subduction rollback. Tectonophysics 445: 245-272.

Mehnert, K.R. 1968. Migmatites and the origin of granitic rocks. Elsevier Pub. Co., 393 p., Ámsterdam.

Nullo, F.E. 1978. Descripción Geológica de la Hoja 41d, Lipetrén, Provincia de Río Negro (1:200000). Servicio Geológico Nacional, Boletín Nº 158, 88 p., Buenos Aires.

Ostera, H., Linares, E., Haller, M., Cagnoni, M. y López de Luchi, M.G. 2001. A widespread Devonian metamorphic episode in northern Patagonia, Argentina. En Tomlinson, A. (ed.) 3º South American Symposium on Isotope Geology, Abbreviated Abstracts Volume, Revista Comunicaciones 52:160.

Page, R. y Page, S., 1993. Petrología y sugnificado tectónico del Jurásico volcánico del Chubut central. Revista de la Asociación Geológica Argentina 48: 41-58.

Pankhurst, R.J., Rapela, C.W., Fanning, C.M. y Marquez, M. 2006. Gondwanide continental collision and the origin of Patagonia. Earth Science Reviews 76: 235-257.

Passchier, C.W. y Trouw, R.A.J. 2005. Microtectonics, Springler Verlag, 366 p., Berlin

Paterson, S. R. 2009. Magmatic tubes, pipes, troughs, diapirs, and plumes: Late-stage convectiveinstabilities resulting in compositional diversity and permeable networks in crystal-rich magmas of the Tuolumne batholith, Sierra Nevada, California. Geosphere 5: 496-527.

Paterson, S.R., Fowler Jr., T.K., Keegan, L.S, Yoshinobu, A.S., Yuan, E.S. y Miller, R.B., 1998. Interpreting magmatic fabric patterns in plutons. Lithos: 44: 53-82.

Paterson, S. R., Vernon, R. H. y Tobish, O. T. 1989. A review of criteria for the identification of magmatic and tectonic foliations in granitoids. Journal of Structural Geology 11: 349-363.

Pignotta G.S., Paterson S.R, Coyne C.C, Anderson J.L y Onezime, J. 2010. Processes involved during incremental growth of the Jackass Lakes pluton, central Sierra Nevada batholith. Geosphere 6: 130-159.

Proserpio, C.A. 1978. Descripción Geológica de la Hoja 42d, Gastre, Provincia del Chubut (1:200000). Servicio Geológico Nacional, Boletín Nº 159, 75 p., Buenos Aires.

Rapela, C.W., Dias, G.F., Franzese, J.R., Alonso, G. y Benvenuto, A.R. 1991. El Batolito de la Patagonia central: evidencias de un magmatismo triásico-jurásico asociado a fallas transcurrentes. Revista Geológica de Chile 18: 121-138.

Rapela, C.W. y Pankhurst, R.J. 1992. The granites of northern Patagonia and the Gastre Fault System in relation to the break-up of Gondwana. En Storey, A.T., Alabaster, T. and Pankhurst R. J. (eds), Magmatism and the Causes of Continental Break-Up, Geological Society of London Special Publication 68: 209-220.

Rapela, C.W., Pankhurst, R.J. y Harrison, S.M. 1992. Triassic "Gondwana" granites of the Gastre district, North Patagonian Massif. Transactions of the Royal Society of Edinburgh, Earth Sciences 83: 291-304.

Ravazzoli, I. y Sesana, F.L. 1977. Descripción geológica de la Hoja 41c, Río Chico, provincia de Río Negro (1:200000). Servicio Geológico Nacional, Boletín Nº 148, 80 p., Buenos Aires.

Rochette, P., Jackson, M. and Aubourg, C. 1992. Rock magnetism and the interpretation of anisotropy of magnetic susceptibility. Reviews in Geophysics 30: 209-226.

Tuccillo, M.E., Essene, E.J. y van der Pluijm, B.A. 1990. Growth and retrograde zoning in garnets from high-grade metapelites: Implications for pressure-temperature paths. Geology 18: 839-842.

Varela, R., Basei, M.A.S., Cingolani, C.A., Oswaldo Siga, J. y Passarelli, C.R. 2005. El basamento cristalino de los Andes norpatagónicos en Argentina: geocronología e interpretación tectónica. Revista Geológica de Chile 32: 167-187.

Volkheimer, W. 1964. Estratigrafía de la región extra-andina del Departamento de Cushamen (Chubut), entre los paralelos 42º y 42º 30´ y los meridianos 70º y 71º. Revista de la Asociación Geológica Argentina 20: 85-107.

Volkheimer, W. y Lage, J. 1981. Descripción Geológica de la Hoja 42 c, Cerro Mirador, provincia del Chubut (1:200000). Servicio Geológico Nacional, Boletín 181, 71 p., Buenos Aires.

von Gosen, W. y Loske, W. 2004. Tectonic History of Calcatapul Formation, Chubut Province, Argentina, and the "Gastre Fault System". Journal of South American Earth Sciences 18: 73-88.

Vernon, R.H. 2004. A practical guide to Rock Microstructure. Cambridge University Press, 606 p., Cambridge.

Wheeler, J., Mangan, L.S. y Prior, D.J. 2004. Disequilibrium in the Ross of Mull contact metamorphic aureole, Scotland: a consequence of polimetamorphism. Journal of Petrology 45: 835-853.

Yoshinobu, A. S., Wolak, J. M., Paterson, S. R., Pignotta G. S. y Anderson, H. S., 2009. Determining relative magma and host rock xenolith rheology during magmatic fabric formation in plutons: Examples from the middle and upper crust. Geosphere 5: 270-285.

Zaffarana, C. B. 2011. Estudio de la deformación pre-cretácica en la región de Gastre, sector sur del Macizo Norpatagónico. Doctoral Thesis, Universidad de Buenos Aires (unpublished) 380 p., Buenos Aires.

Zaffarana, C.B., López de Luchi, M.G., Somoza, R., Mercader, R., Giacosa, R. y Martino, R.D. 2010. Anisotropy of magnetic susceptibility study in two classical localities of the Gastre Fault System, central Patagonia. Journal of South American Earth Sciences 30: 151-166.

Zaffarana, C.B. y Somoza, R. 2012. Palaeomagnetism and $^{40}Ar/^{39}Ar$ dating from Lower Jurassic rocks in Gastre, central Patagonia: further data to explore tectonomagmatic events associated with the break-up of Gondwana. Journal of the Geological Society, London, doi:10.1144/0016-76492011-089.

Žák, J., Paterson S.R y Memeti V. 2007. Four magmatic fabrics in the Tuolumne batholith, central Sierra Nevada, California (USA): implications for interpreting fabric patterns in plutons and evolution of magma chambers in the upper crust. Geological Society of America Bulletin 119: 184-201.

Žák, J., Holub F.V. y Kachlík V. 2006. Magmatic stoping as an important emplacement mechanism of Variscan plutons: evidence from roof pendants in the Central Bohemian Plutonic Complex (Bohemian Massif). International Journal of Earth Sciences 95: 771-789.

Žák, J., Schulmann K. y Hrouda F. 2005. Multiple magmatic fabrics in the Sázava pluton (Bohemian Massif, Czech Republic): a result of superposition of wrench-dominated regional transpression on final emplacement. Journal of Structural Geology 27: 805-822.

Recibido: 17 de agosto, 2011.
Aceptado: 5 de marzo, 2012.